Boom and Bust: Investigative Seismology in Cheverly, Maryland

Resolution of Booms by Use of a Seismic Nodal Array

Prepared For: Geology 394 - Senior Thesis II

By: Peter Meehan

Advisor: Vedran Lekic Ph.D.

22 November, 2017

TABLE OF CONTENTS

I. Abstract

Array seismology is a tool utilized to locate and identify the sources of ground waves. Though initially used to differentiate between waves emitted by nuclear explosions and those from earthquakes, seismological analysis has recently been able to identify sources of unusual seismicity as well as anthropogenic noise. In this study, I collected and analyzed seismic data to identify the source of distressing loud boom events reported by residents of the town of Cheverly, Maryland. Previous studies of similar booms led seismologists to identify local seismicity beneath Moodus, Connecticut. However, anthropogenic acoustic sources, such as the Carlsbad pipe explosion in 2002, can also produce seismic waves. Therefore, in this work, I carry out a suite of analyses to ascertain the severity of the reported booms and analyze their seismic signatures. I start by collecting descriptive survey data on boom occurrences in Cheverly, and translate them to a quantitative view through the modified Mercalli Intensity Scale. Based on this preliminary analysis, I formulate the hypothesis that the Cheverly booms are produced by local earthquakes. To test this hypothesis, I deployed an array of fifteen, three component seismometers, which recorded four reported booms. I analyze seismic records gathered by the array to identify the spectral characteristic of the waveforms associated with the Cheverly booms, and find that the waveforms are nearly indistinguishable from boom to boom, suggesting that they have a common origin and that they are co-located to within less than 25 meters distance. By analyzing the relative arrival times of the seismic waves across the array, I determine that the velocity of the waves is consistent with sound propagating in air and inconsistent with seismic waves traveling through the ground. Furthermore, I find that a source at the surface provides a better fit to the data than does a source at depth. Based on these findings, I reject my initial hypothesis, and formulate the hypothesis that the booms originate at a local recycling plant. I then use the relative arrival times of waveforms associated with the booms to locate their origin within Joseph Smith and Son's Professional Services, and validate this location by performing a polarization analyses. Finally, by considering the constraints of scope for this project's analysis in contrast to the extensive data source, I explore possibilities for follow-up investigations.

II. Introduction

Array Seismology

Array seismology evolved in the 1960s primarily to identify nuclear detonations, with work focused on noise elimination and seismic signal maximization (Husebye and Ruud, 1989). An array is composed of multiple seismometers, arranged with specific orientation and spacing. When discussing seismic arrays, this paper will use the terms "node" and "instrument" interchangeably to refer to an individual seismometer. Recordings from seismometers are filtered using low pass filters to suppress noise and isolate the source signals.

Sounds Associated With Earthquake

Observers of earthquakes often report hearing the event prior to feeling the vibrations. In his report of the 1906 California Earthquake, Lawson describes the common experience of hearing rumbling sounds in association with the earthquake (Lawson, 1908). However, these reports are largely descriptive in nature, and therefore, have scarce associated quantitative record.

On the basis of prolific descriptive reports such as those of the 1906 California Earthquake, Hill et al. 1976, examined the potential of seismic activity of to produce audible sound prior to observable ground vibration. By comparing acoustic waves to seismic waves for three low magnitude, localized earthquakes, Hill et al. indicate consistency between spikes in acoustic recordings in the range of 50 Hz to 70 Hz and the arrival of P waves (Hill et al., 1976). P waves usually express less energy than S waves (Boatwright & Fletcher, 1984), and therefore, the ground vibration associated with P waves is likely more challenging for the lay observer to perceive. Given that the perceptive hearing of humans ranges from 31 Hz to 17.6 kHz (Heffner, 2007), the findings of Hill et al. suggest that the sound waves produced upon P wave arrival are within a range perceivable by the human observer. Therefore, the reports of sounds prior to the observation of earthquake ground vibration is a result of acoustic waves produced upon the arrival of P wave energy.

III. Background

Regional Overview

Cheverly is a town located in Prince George's County, Maryland, adjacent to the northeastern border of Washington D.C. The town is 3.29 square kilometers in area with a population of 6,173 residents as reported by the 2010 U.S. Census (Town of Cheverly).

The town lies primarily on lower Cretaceous sand-gravel and silt-clay facies of the Potomac Group. The southwestern corner of the town lies on Quaternary Alluvium deposits (Glaser, 2003). See **Figure 3.1** for a map of Cheverly.

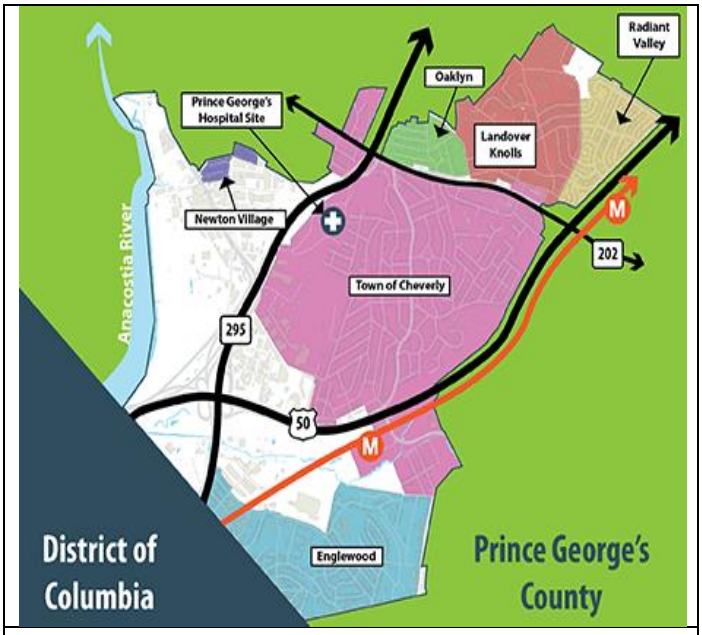

FIGURE 3.1 - The above map, adapted from the Greater Cheverly Sector Plan, developed by Prince Georges County Planning Department, shows the extent, and relative zoning of Cheverly, MD.

Problem Overview

Since 2008, residents of the Town of Cheverly have reported loud events, referred to as booms due to their low-pitched characteristics. These booms continue to disturb residents and concern local government. Because of heightened concern, the mayor of Cheverly, Mike Callaghan, contacted the University of Maryland Seismological Laboratory for consultation.

Preliminary Surveys

Loudness as well as geographic and time distribution of the Cheverly booms were interpreted with the use of an online reporting form for residents to report boom observations. From mid-December 2016 through March 2017, there were more than 190 submitted reports. **Figure 3.2** shows a map of boom reports across Cheverly. Individual reports are color coded by their qualitative reported intensity. These preliminary data directed the placement of instruments across Cheverly. Furthermore, access to the online reporting tool by residents was available through the duration of seismic data collection. Reports submitted during the span of seismic data collection helped to screen data for boom occurrence.

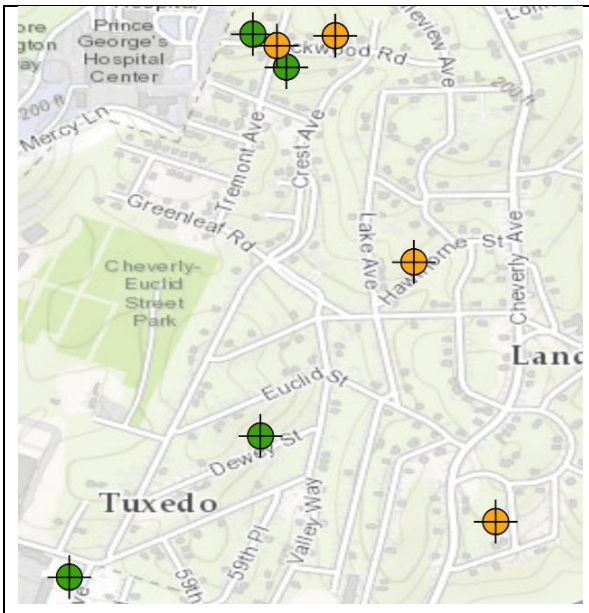

December 21st 2016

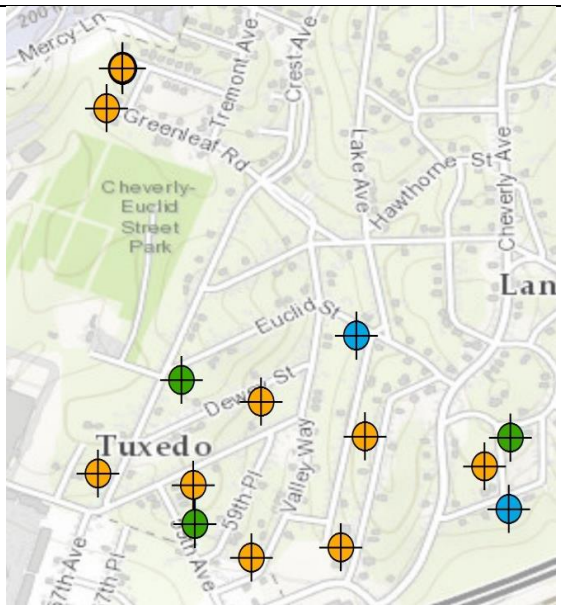

January 19th 2017

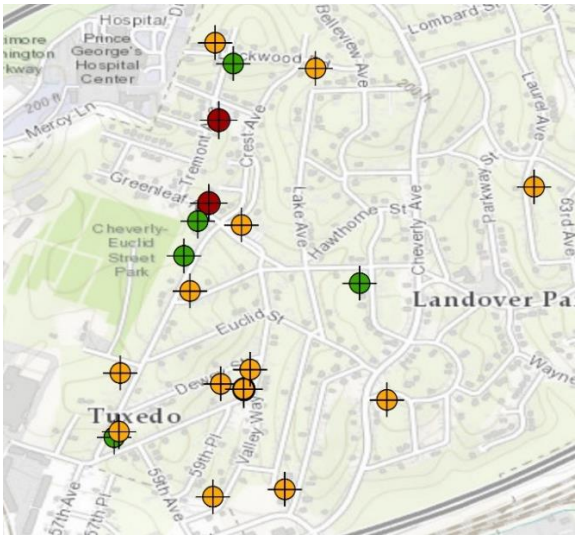

January 31st 2017

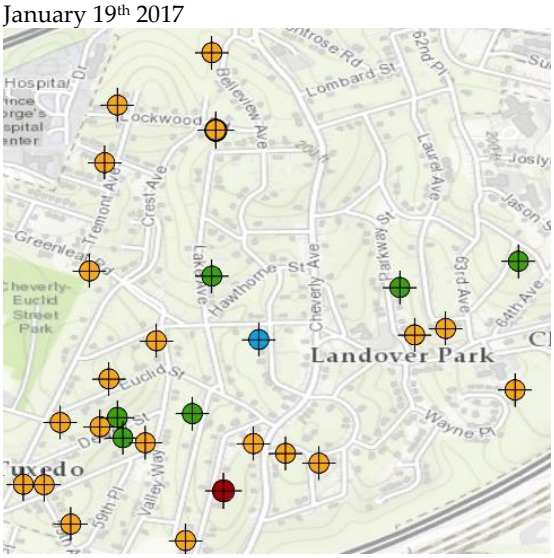

March 21st 2017

FIGURE 3.2: Distribution of boom events, as reported by the residents of Cheverly, MD from December 2016 – March 2017. The individual events are color coded by their reported loudness.

Barely Audible – Deafeningly Loud

Event Intensity

The Modified Mercalli Intensity Scale establishes a standard of evaluating earthquake intensity by the descriptive reports of observers. The following are the standards for an intensity II and Intensity III earthquake as set forth by Wood 1931:

II. Felt indoors by few, especially on upper floors, or by sensitive, or nervous persons. Also, as in grade I, but often more noticeably: sometimes banging objects may swing, especially when delicately suspended; doors may swing, very slowly; sometimes birds, animals, reported uneasy or disturbed; sometimes dizziness or nausea experienced.

III. Felt indoors by several, motion usually rapid vibration. Sometimes not recognized to be an earthquake at first. Duration estimated in some cases. Vibration like that due to passing of light, or lightly loaded trucks, or heavy trucks some distance away. Hanging objects may swing slightly. Movements may be appreciable on upper levels of tall structures. Rocked standing motor cars slightly (Wood, 1931).

Preliminary descriptive reports are congruent with the descriptions of low intensity earthquakes. Of the 190 residential reports from Cheverly Maryland, 78.4 percent reported objects such as windows and cabinets rattling. Of these reports, eleven descriptions explicitly compared the event to a truck or train collision. The recurring descriptions of houses shaking, windows rattling, alarms being set off, and objects vibrating are consistent with that of an event between II and II on the Modified Mercalli Intensity Scale.

Objective

Based on the preliminary reporting by residents, I find reports of Cheverly booms to be consistent with a seismic event of intensity II or II on the modified Mercalli Intensity scale. This project seeks to falsify the hypothesis that booms observed in Cheverly, Maryland are a manifestation of the P wave arrival from shallow, localized earthquakes. Evidence including inconsistent wave velocity, isometric first motion, and a shallow or surficial depth of origin will falsify the hypothesis. Should the initial hypothesis be falsified, the project will view data through the lens of a secondary hypothesis. This secondary hypothesis is that booms found not to be seismic in nature, originate from industrial recycling facilities located within 2000 meters to the south west of Cheverly.

IV. Experiment Design

Deployment

Twenty-two seismic nodes, divided into two sub-arrays, were deployed throughout Cheverly, Maryland. Sub-array 1, consisting of fifteen nodes, acquired data for thirty-five days, from March 22nd 2017 through April 26th 2017. Sub-array 2, consisting of seven nodes placed redundantly at sites of Sub-array 1, acquired data from March 22nd through April 5th. The fourteen days of continuous seismic data collected by sub-array 2 was used as a trial set for preliminary analysis. Due to redundancy of data, this paper will not discuss data collected by sub-array 2.

Deployment was accomplished with assistance from the following members of the University of Maryland Seismological Laboratory: Scott Burdick Ph.D., Erin Cunningham, and Phillip Goodling. For deployment, instruments were buried in holes of approximately fifteen centimeters width and thirty centimeters depth. Nodes were oriented with their north-south component due north for the sake of consistent directional interpretation.

Instrumentation

This project used Fairfield Nodal - ZLand 3C seismic nodes to acquire seismic data. These instruments are three channel seismometers, which record ground vibrations in two orthogonal horizontal and one vertical directions, by means of three geophones. An individual data set is recorded for each direction of vibration, as such, I will use the term "component" in reference to the data provided by a single geophone within the seismometer.

Data are sampled at an interval of two milliseconds, with a timing accuracy of ± 10 microseconds. The ZLand 3C is a cordless unit, which records continuous data for up to thirty-five days, maintaining timing accuracy via GPS satellites, even when buried. A Hand Held Transmitter (HHT) loads specific data collection schemes onto each instrument. Data acquisition commences only once the node passes three deployment tests: an impedance test, a step test, and a resistance test. Prior to data acquisition, each instrument records the coordinates of the deployment location via GPS satellites.

Array Orientation

Deployment locations were selected based on the following factors: concentration of event reports, distance from main roads, railroads, and other high traffic features,

distance of separation between individual nodes, and permission of the property owner of the desired location.

Residential reports indicated booms to be audible, thereby implying that events must occur within low frequencies of approximately 20 Hz to 200 Hz. Under the assumption of a P wave velocity through sand/silt facies of approximately 2000 m/s (Bourbie et al., 1987), the maximum wavelength expected was 100 meters. This wavelength was accommodated by arranging each node of the array with an irregular spacing of approximately 100 meters.

The ability to determine slowness vector (angle of incidence) and back azimuth depends on observation of different arrival times of the wave front to individual seismometers (Rost and Thomas, 2002). A linear arrangement of nodes enables clear observation of apparent velocity, should the wave propagate parallel to the trend of the array (Rost and Thomas, 2002). However, should the wave propagate perpendicular to the linear array, apparent velocity would be impossible to discern, as arrival times at each node would be simultaneous. As such, the array contained an arrangement of two, crossing lineations, such that waves propagating from any direction would experience different arrival times at each seismometer.

Array Geometry

To maximize the arrival time difference and to accommodate the north and south foci of reports, I arranged the array to form three linear segments. One linear arrangement, referred to as Line 1, contained nodes 1 through 6, which extend from the southern extent of Cheverly to the northern extent. Two separate linear arrangements, referred to as Line 2 and Line 3, contained nodes 7 through 10, and 11 through 15, respectively. Line 2 crossed Line 1 at a near perpendicular angle in the southern extent of Cheverly, and Line 3 crossed Line 1 at a near perpendicular angle in the northern extent of Cheverly. The distribution of deployment locations across Cheverly is displayed in **Figure 4.1**.

The majority of property in Cheverly Maryland is privately owned, requiring the permission of each property owner for deployment. With the assistance of the mayor of Cheverly, permission was requested from the property owner of each desired location. Only three locations were adjusted to adjacent properties due to unwillingness of the property owner to host a seismometer.

Each node was connected to the Hand Held Transmitter in order to initiate deployment tests; upon the condition that the node passed all deployment tests, data acquisition commenced. Seismometers were retrieved at the end of the deployment duration and continuous data harvested.

FIGURE 4.1 - This map shows the 16 deployment locations of seismic nodes. Six of these locations contained two nodes, one from the sample group and one from the full duration group. These locations express a blue and a green triangle

V. Methods of Analysis

Analysis of collected seismic data consists of two processes, event identification and calculation of event source location. The data are continuous and span a duration of multiple weeks. Mere data quantity encumbered computer programs utilized for analysis such as Python and MATLAB. In order to identify windows of interest, residential boom reports were viewed in parallel to seismic data.

Event Identification

The first of these steps is event identification; the screening and filtering of the seismic record in comparison with residential reports, in order to identify the occurrence of an event. Event identification involves plotting vertical component seismograms from each of the fifteen nodes across the array and creating time-frequency spectrograms. I apply sixth order low pass filters, at 50 and 100 Hz, through which any boom signatures can be seen within seismograms. Booms are initially identified when an anomalous, isolated, and coherent wave is observed across the array at the time targeted by residential reports.

After initially identifying a boom within the seismograms, I created spectrograms to express signal power across the range of filtered frequencies for the given window of interest. These visualizing these spectrograms enables quick comprehension of peak frequencies and event timing. Booms are confirmed when an isolated, low frequency burst was observed at the target time identified within seismograms.

Event Location

The propagation of a wave can be defined by two parameters: the vertical incident angle (slowness vector), *i*, and the back azimuth θ. (Rost and Thomas., 2002). These parameters are illustrated in **Figure 5.1**, adapted from Rost and Thomas, 2002. The first stage of identifying event location involves the calculation of back azimuth θ as an aggregation of instantaneous particle motion strike calculations.

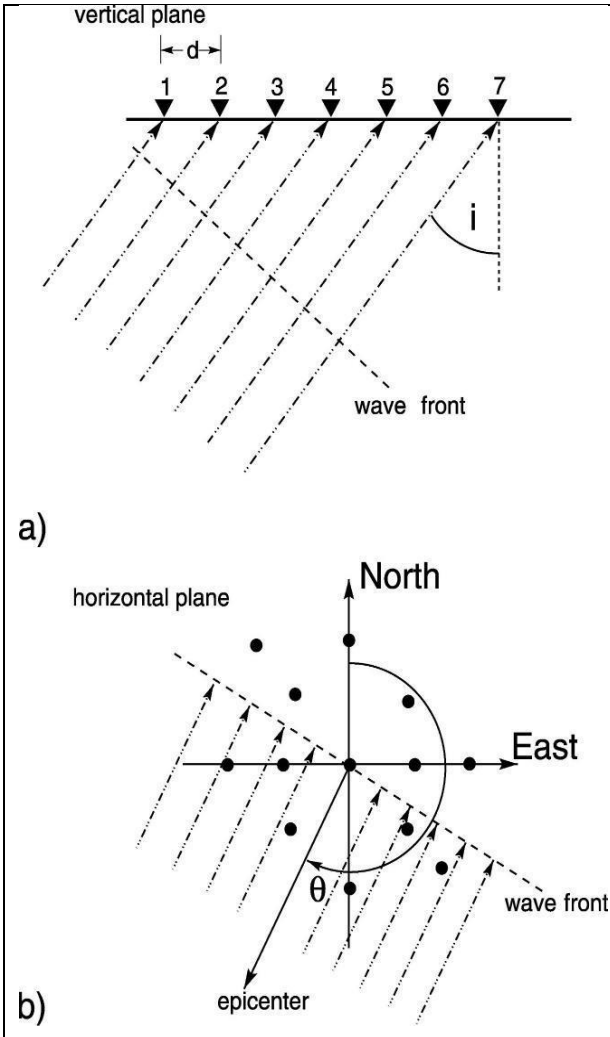

Figure 5.1 - Adapted from Rost 2002. Vertical and Horizontal components of a wave as they relate to node placement within an array.

I evaluate three-dimensional particle motion at each station, during the wave onset interval by using instantaneous polarization analysis. For the purpose of this paper, the term wave onset interval will refer to the duration within the seismic record between the wave arrival, and moment of maximized phase envelope. The phase envelope, which describes the compounded wave amplitudes from each component, is crucial in identifying time frames in which signal to noise ratios are maximized and waveform most isolated for analysis. The interval from wave onset to maximized envelope has been chosen for analysis in order to limit the influence of sound reverberation. As residents report audible observations of booms, we can infer that booms involve the propagation of sound waves accompanied by multi-directional reverberation from echoes. The identified wave onset interval has been chosen as the primary scope of particle motion analysis in order to minimize the influence of these reverberations within estimation of source direction.

This project follows the instantaneous polarization methods of Morozov and Smithson, 2008. This method calculates the strike of particle motion in accordance to sampling frequency, which, in the circumstance of this experiment, is every 2 milliseconds. This method provides two calculated back azimuths, one appropriate for when particle motion is primarily linear, and one for when particle motion is primarily elliptical. The orientation of these back azimuths are referred to as Strike A and Strike P respectively. This paper has utilized Strike P for aggregated back azimuth plots, as I found particle motion to have elevated ellipticity during moment of maximum phase envelope. An expression of this ellipticity is seen within **Figure 5.9**. This figure first plots the three component particle motion with respect to time as shown by color. It then plots the combined phase envelope verses time. Finally, the figure expresses calculated ellipticity, which is seen to maintain high values during and just after the phase envelope is maximized.

I represent the set of calculated back azimuths as a plot of vectors, with direction determined by calculated strike, and magnitude determined by density of back azimuths occurring within a bin range of (+/-) three degrees. Through this method, mean back azimuth and variance are represented for each station. I then view distribution of back azimuths for each station across the array in order to project a generalized direction to possible source locations. This method lacks precision to isolate source location alone, however, it constrains direction to source, thereby verifying or rejecting results from further location analysis.

Determination of event source location requires the manual picking of wave front, or phase, arrival times within the seismic record of each station. Following procedures of Diehl & Kissling 2002, phase arrival is defined as a change primary amplitude beyond that of background noise (ASNR), or a change in dominant frequency in contrast to that of background noise (FSNR). By defining known node locations associated with arrival times, apparent wave velocity across the array is calculated (Rost and Thomas, 2002). The triangulation of these velocity vectors identifies a point of origin.

VI. Presentation of Data

Review of the 35 day seismic record observed of four booms. Each was reported by more than six residents, with consistent timing between reports. These events occurred on April 2 at 6:17 UTC, April 9 at 12:50 UTC, April 14 at 7:09 UTC, and April 24 at 3:47 UTC. Additionally, an earthquake, occurring on March 29th at 4:09 UTC, was used for the analysis of uncertainty.

Event Identification By Seismogram

Seismic data from the deployed array were windowed to timeframes enveloping the time reported by residents. A sixth-order low pass filter at 100 Hz was applied to the data of each targeted timeframe. When seismograms of each station are plotted, we see a distinct, coherent waveform recorded across the array.

Data for the April 2nd event were taken from a trace which began at 06:00 UTC. **Figure 6.1** shows a 20 second segment of this trace with the vertical-component from each of the 15 stations plotted. The waveform's arrival at the first station is seen at 1022 seconds on the trace, or 06:17:02 UTC. This is precisely when residents identified a boom to have occurred. Therefore, a 500 second target window from 750s to 1050s was for further spectrogram analysis.

Data for the April 9th event were taken from a trace with start time of 0:00 UTC. When windowed to view the reported time, a coherent waveform is seen across all stations. Plots of the amplitude of vertical vibration from each of the 15 stations can be seen in **Figure 6.2.** With a first arrival time of 46170 seconds, or 12:49:30 UTC, this signal occurs within 30 seconds of the reported boom time given by residents. Consistency in timing and the coherency in waveform guided the selection of a 500 second target window from 45900 seconds to 46400 seconds for spectrogram verification.

Seismic recordings for the event reported on April 14th begin at 06:30 UTC April 14th. By filtering as described with the previous events, and windowing to the timeframe directly before and after the targeted time of 7:09 UTC, a waveform is observable across all stations in the array. Within the vertical components of all stations, plotted in **Figure 6.3**, this waveform is observed to have a first arrival time of 2208 seconds, or 7:06:48 UTC which places the arrival time is within three minutes of the residential reported time. This project considers a variance of three minutes to be well within the uncertainty of residential reports given the early hour of the morning and lack of precision in residential

time recording. To verify this event, a 500 second target window from 2000 seconds to 2500 seconds was defined for the plotting of a spectrograms.

The data evaluated for the final event, reported on April 24th, are taken from a trace which begins at 0:00 UTC April 24. After appropriate windowing and filtering as described in previous events, a coherent wave is seen across all stations. The vertical components of the fifteen deployed stations are plotted in **Figure 6.4**. These vertical vibrations express a first wave onset time of 13679 seconds, or 03:47:52 UTC. Given the consistency to within three minutes of residential reports, a 500 second target window from of 13450 seconds to 13950 seconds is selected for the verification of this event by spectrograms.

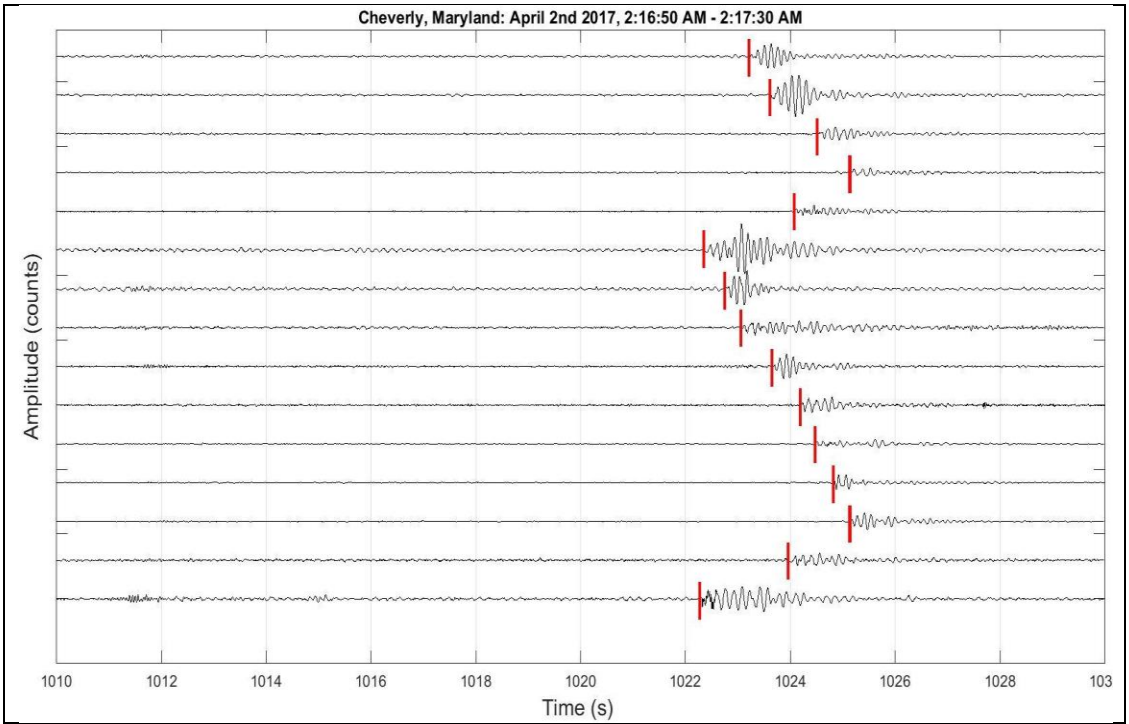

Figure 6.1: The above seismogram plots the vertical component of each of the fifteen deployed stations. A coherent wave is seen arriving at 1022s. The picked arrival times at each station are marked in red.

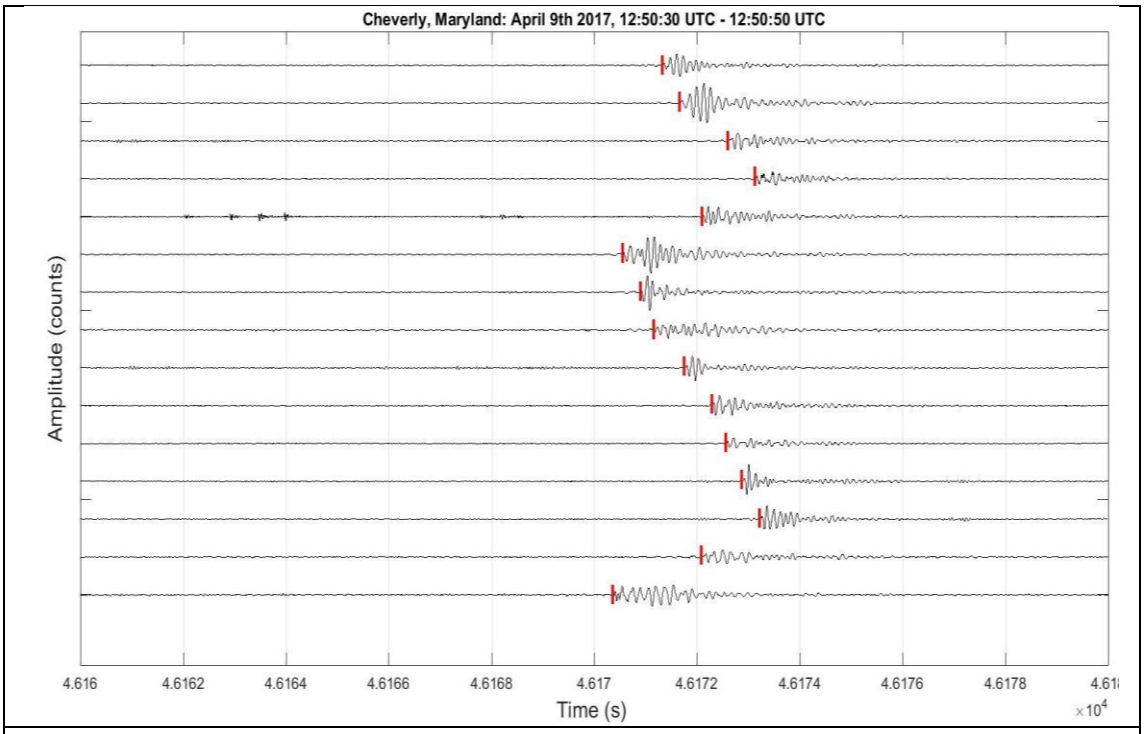

Figure 6.2: The above seismogram plots the vertical component of each of the fifteen deployed stations. A coherent wave is seen arriving at 46170s. The picked arrival times at each station are marked in red.

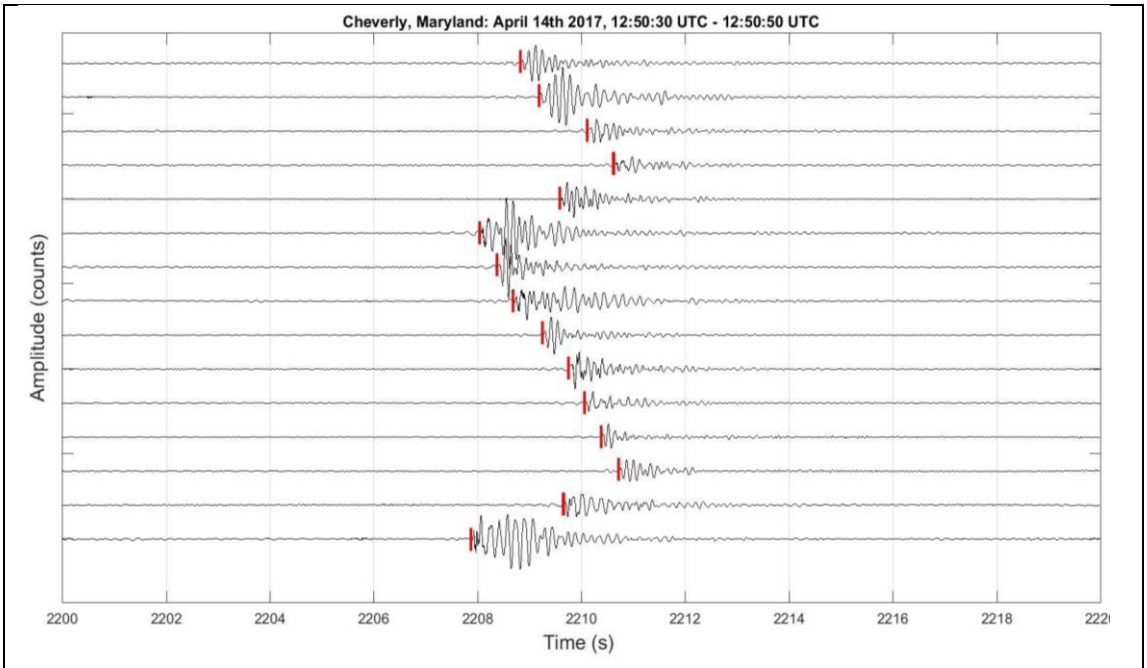

Figure 6.3: The above seismogram plots the vertical component of each of the fifteen deployed stations. A coherent wave is seen arriving at 2208s. The picked arrival times at each station are marked in red.

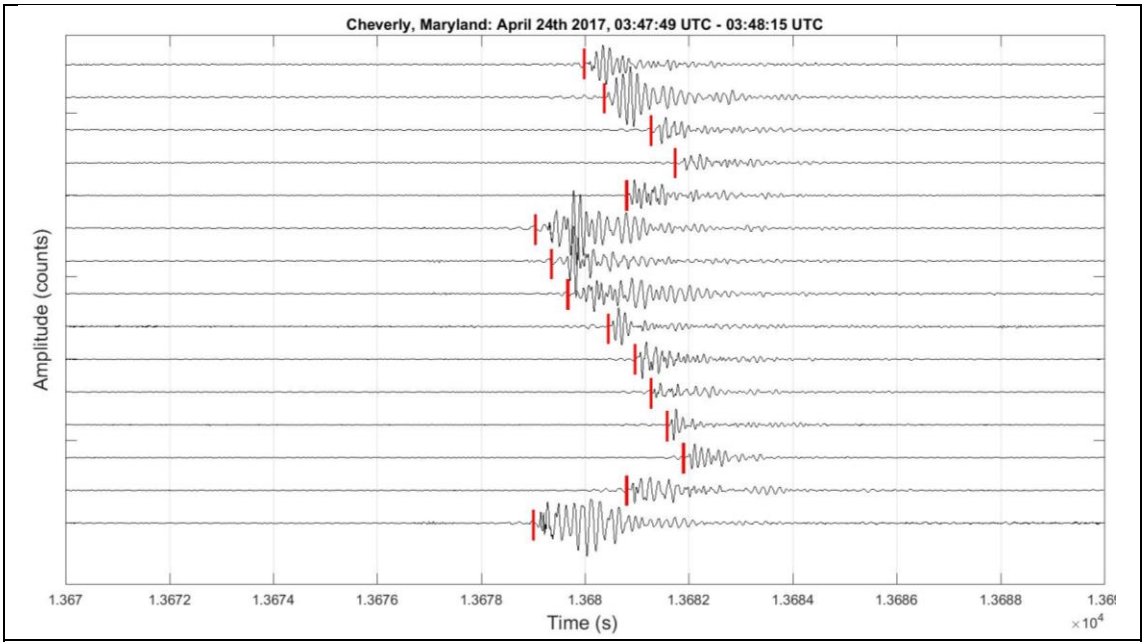

Figure 6.4: The above seismogram plots the vertical component of each of the fifteen deployed stations. A coherent wave is seen arriving at 13679s. The picked arrival times at each station are marked in red.

Event Confirmation by Time-Frequency Analysis

The events identified within seismograms are analyzed using spectrograms. This method of plotting signal power across a range of frequencies with respect to time enables visual interpretation of the character and nature of a signal. These signatures may not be evident in the timeseries themselves due to signals at some frequencies drowning out those at other frequencies. **Figures 6.5, 6.6, 6.7, and 6.8** show the spectrograms for the events of April 2nd, April 9th, April 14th, and April 24th respectively. Each spectrogram is color coded with respect to recorded vibrational power at the given time for the associated frequency, with blue expressing less spectral power, and yellow expressing greater spectral power. **Figures 6.5-6.8** also contain a representative seismogram above the spectrograms for the sake of timing comparison. Within each spectrogram, we see an anomalous burst in low frequency energy, with maximum spectral power at 7 Hz, occurring at the precise time of the waveform's arrival in the seismograms. These anomalous bursts are circled in red within each spectrogram.

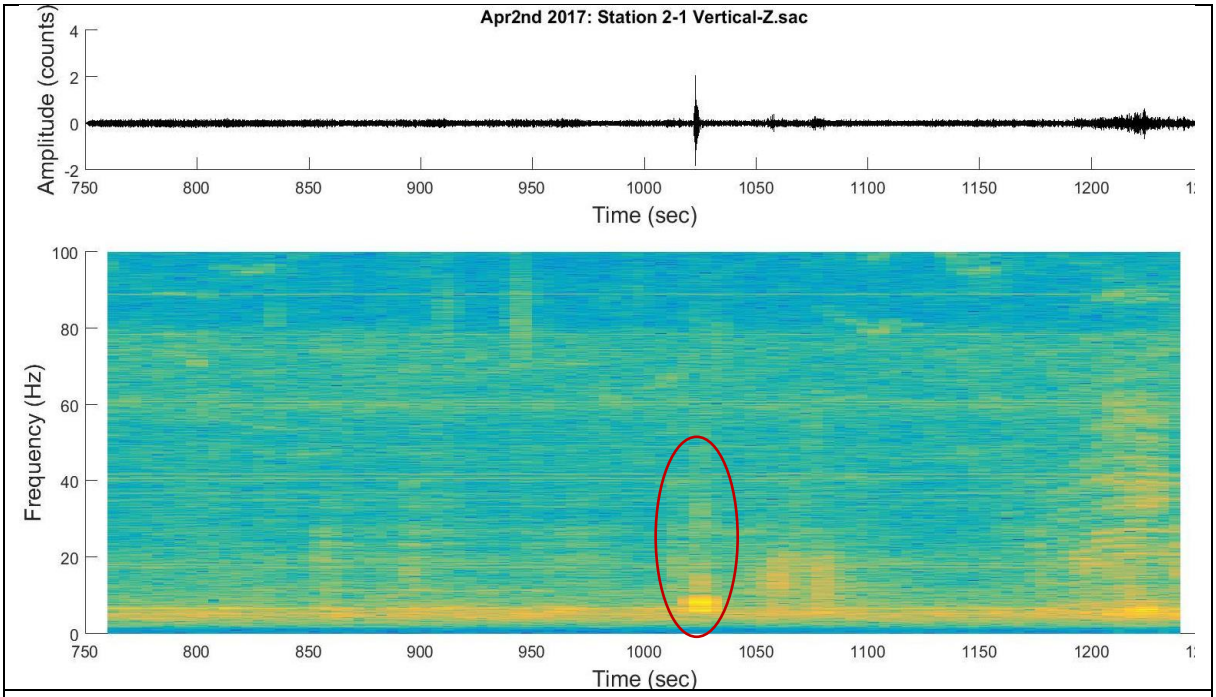

Figure 6.5: The above spectrogram for April 2nd, color coded according to signal power, sees a low frequency burst at 1022s, aligning with residential reports and confirming the event.

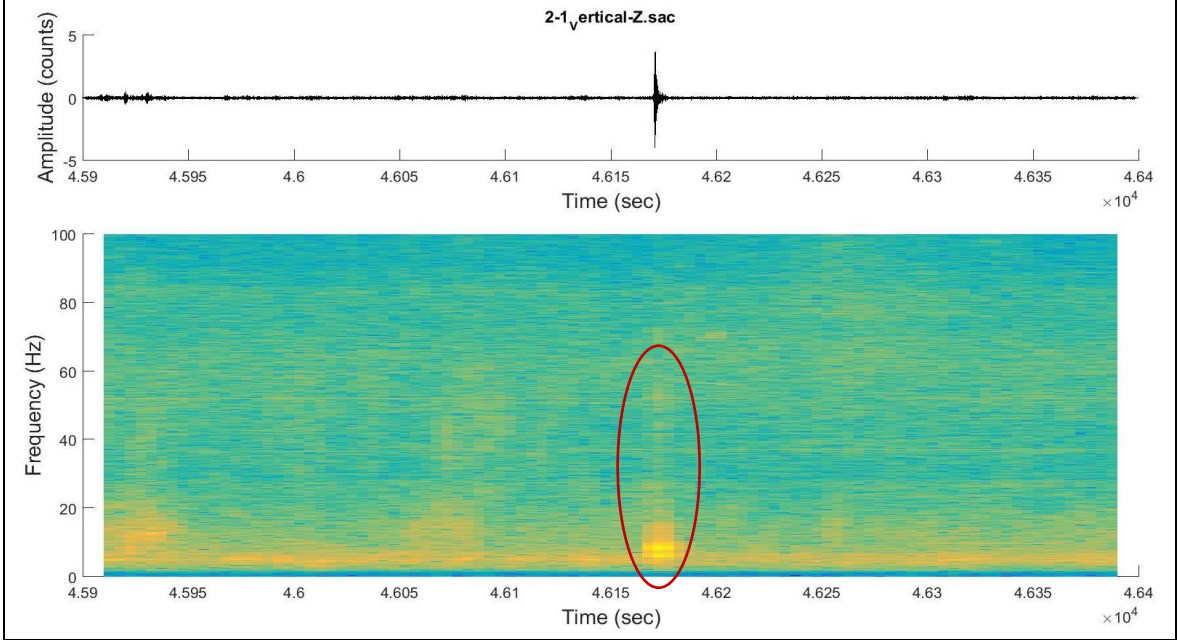

Figure 6.6: The above spectrogram for April 9th, color coded according to signal power, sees a low frequency burst at 46170s, aligning with residential reports and confirming the event.

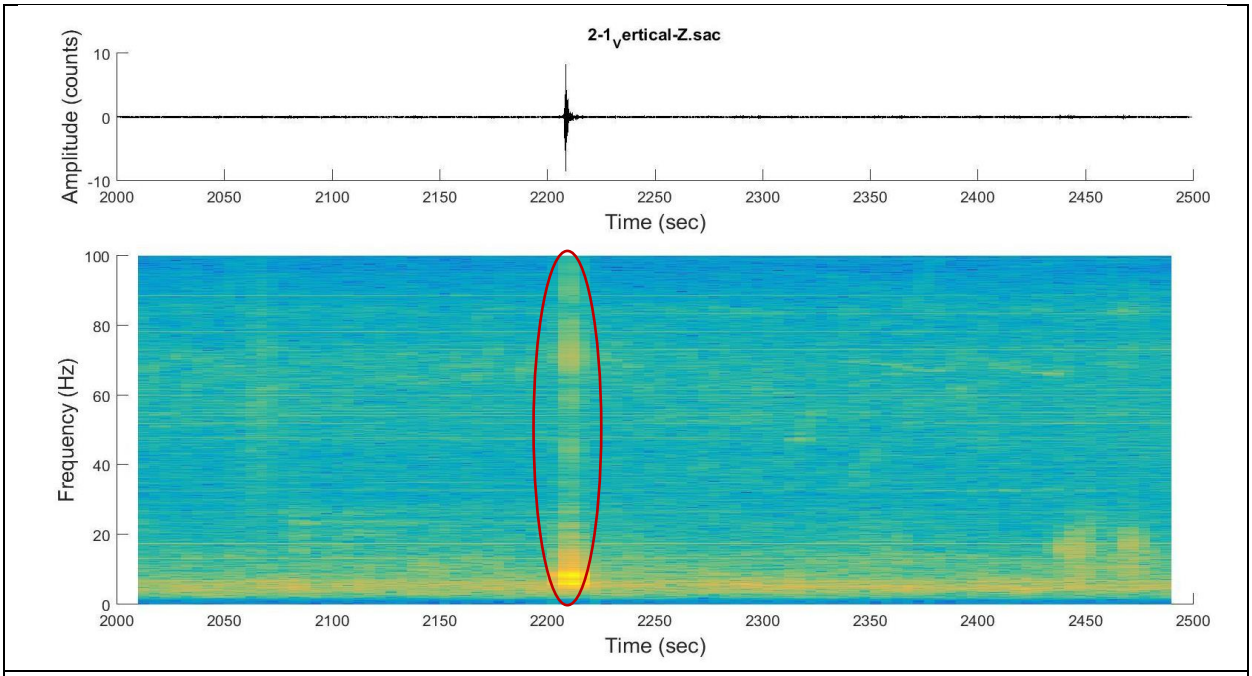

Figure 6.7: The above spectrogram for April 14th, color coded according to signal power, sees a low frequency burst at 2208s, aligning with residential reports and confirming the event.

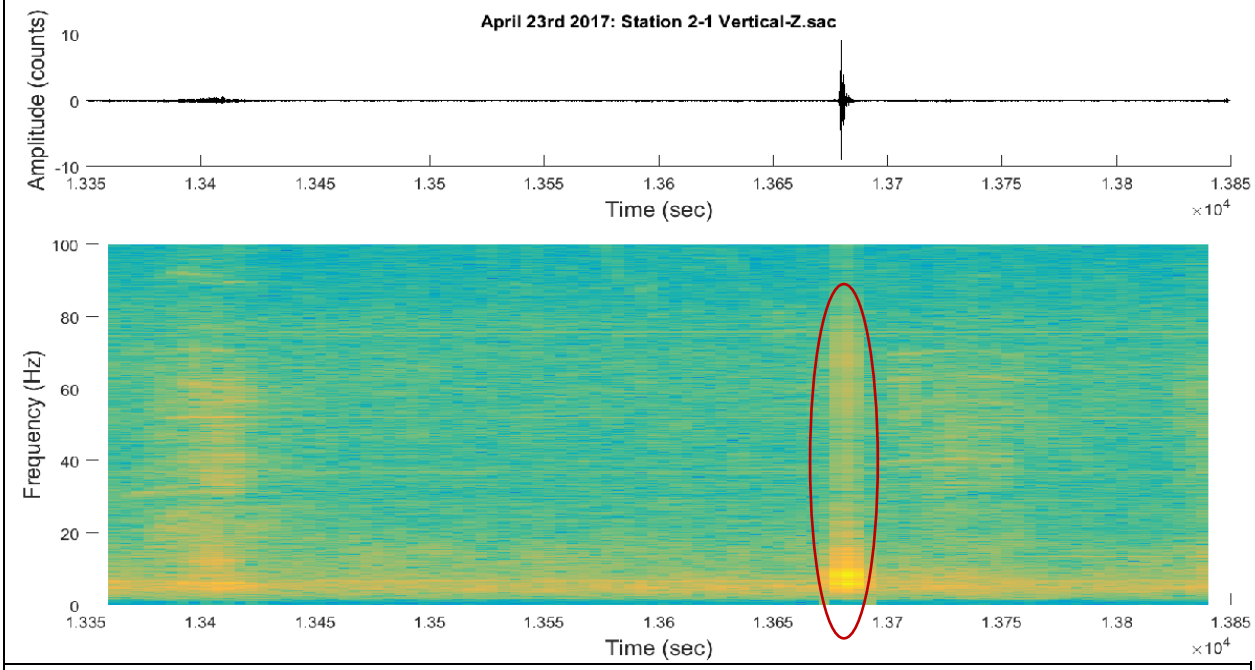

Figure 6.8: The above spectrogram for April 24th, color coded according to signal power, sees a low frequency burst at 13679s, aligning with residential reports and confirming the event.

Direction to Source by Polarization

As stated in methods, I use calculated back azimuth appropriate for intervals of elliptical particle motion. Though waveforms expressed linear tendencies within preliminary onset, notable ellipticity is present during moment of maximized envelope and the duration directly following. **Figure 6.9** shows the plots waveform amplitude of each component, phase envelope, and ellipticity of station 7 for the April 9th. This plot sees ellipticity stabilize during and slightly after the moment of phase envelope maximization, thereby supporting my use of strikes appropriate for ellipticity. In order minimize the effect of noise upon the back azimuth analysis, I calculate back azimuths starting .1 seconds prior to the maximized envelope and ending .15 seconds after the moment of maximized envelope at each stations for all events.

When the plots of back azimuth vectors, formed as described in the methods, are placed at their respective station's coordinates, the viewer is able to interpret 2 dimensional direction to source. **Figures 6.11, 6.12, 6.13, and 6.14** contain these aggregated back azimuth array plots for the April 2nd, April 9th, April 14th, and April 24 events respectively.

During onset, there is general agreement of mean back azimuths between stations. A general trend to the southwest is observed. However, mean back azimuths vary with time and geographic distribution, with greatest variance seen in stations 3, 4, 12, and 13. Uncertainties routed in alignment will be discussed in Section 7. Even when including variance of these four stations, a dominant back azimuth is still observed. Uniformity of back azimuths, especially at stations 5, 10, and 14 constrain the direction to source from -100 degrees to -145 degrees.

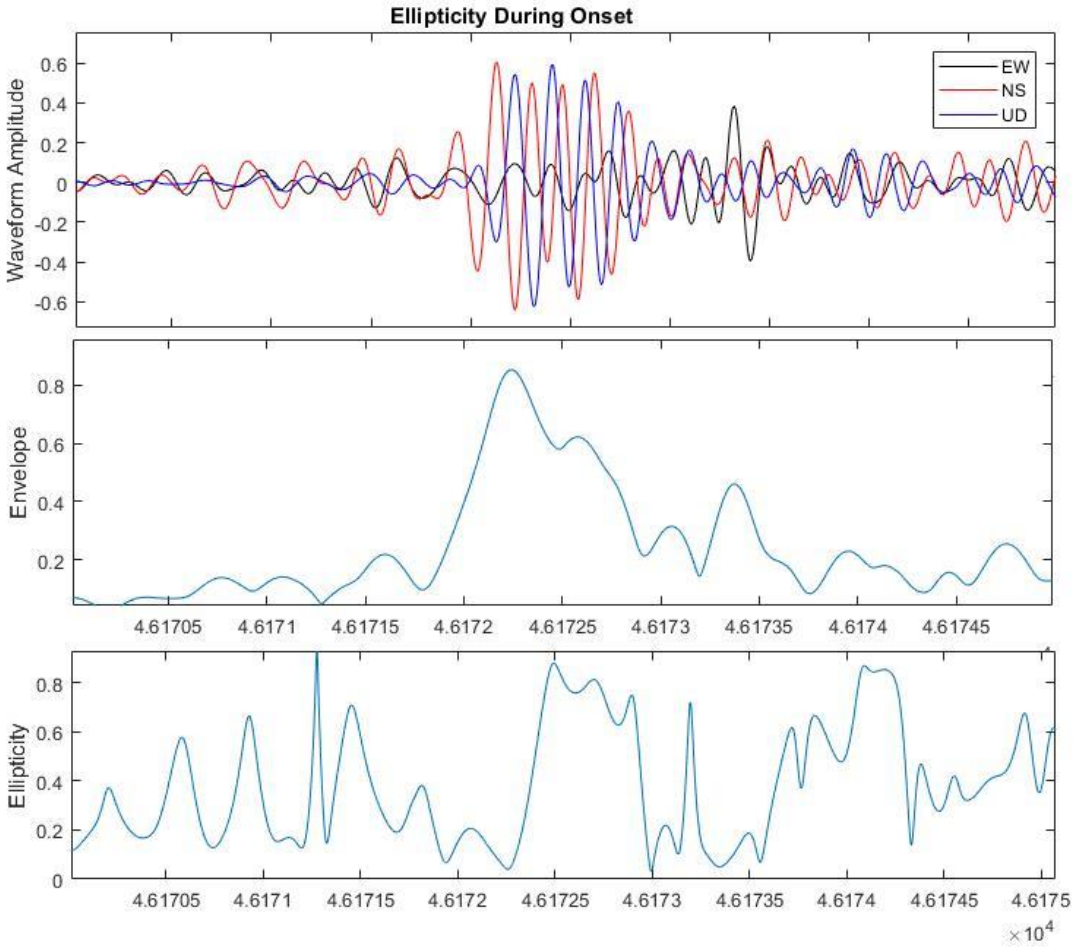

Figure 6.9: Waveform amplitude of each component during wave onset seen with East -West component as black, North-South Component as red, and Up-Down component as blue (top). Phase envelope, derived from aggregated amplitudes, shows maximization during period of highest signal to noise ratio (middle). Ellipticity is seen to maintain high values of greater stability slightly after moment of maximum phase envelope (bottom).

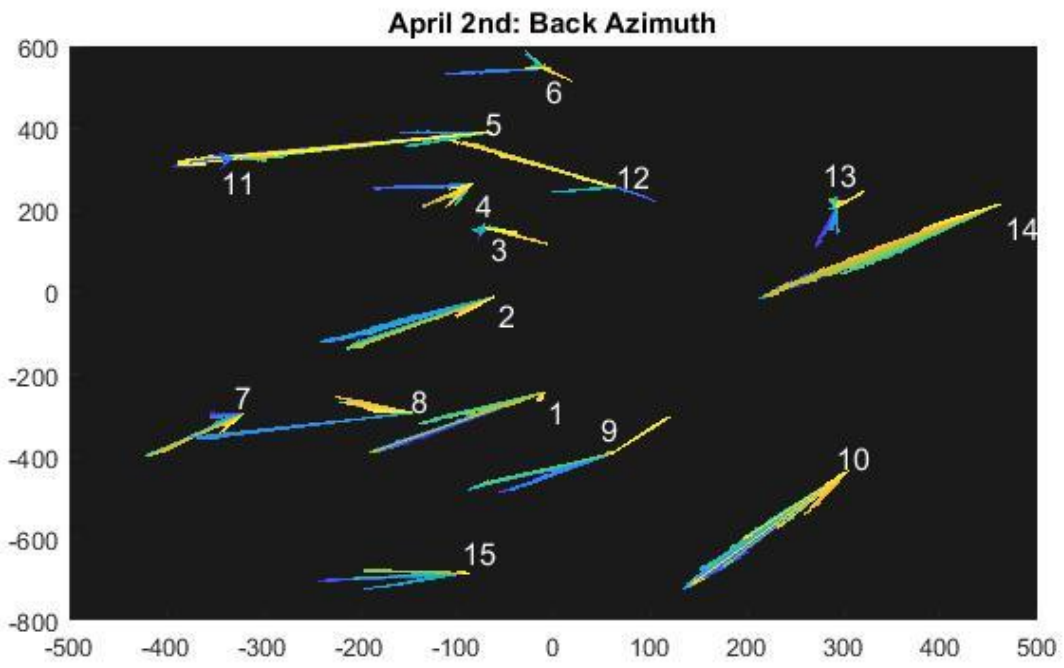

Figure 6.11: The above map plotted back azimuths at each station for the April 2nd event. Azimuths are color coded by time with blue vectors plotted from the initial onset and yellow vectors from the termination of onset at the point of maximized amplitude. Stations are numbered. Note greater variance in Stations 3, 4, 12 and 13. This variance will be resolved in Section 7.

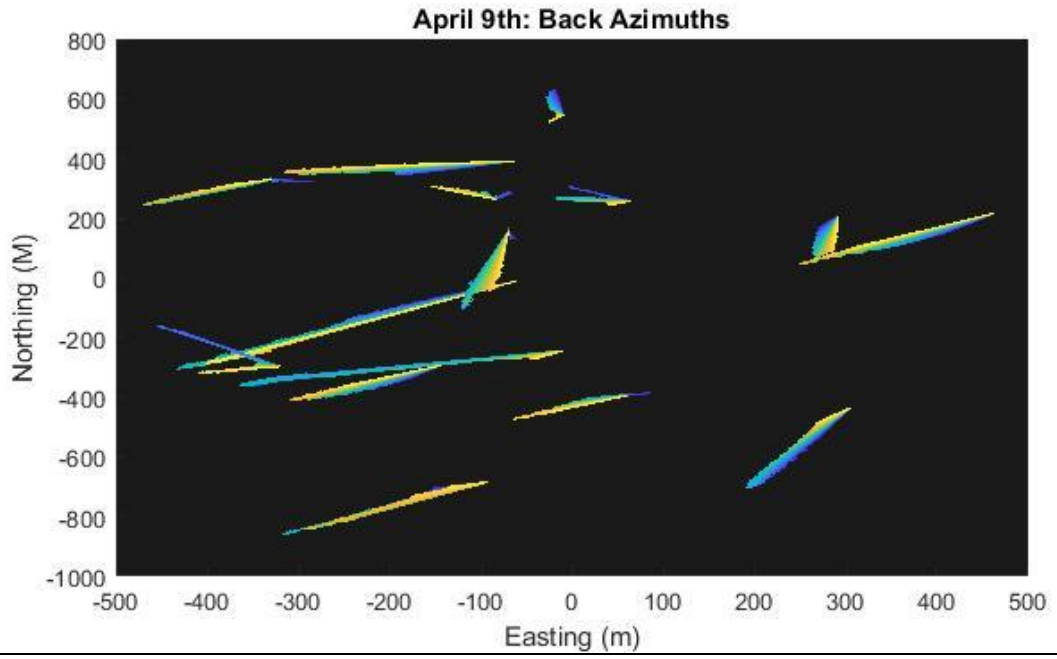

Figure 6.12: Instantaneous back azimuths at each station for April 9th. Azimuths are color coded by time with blue vectors plotted from the initial onset and yellow vectors from just past the point of maximized envelope. Stations with greatest variance remain stations 3, 4, 12 and 13.

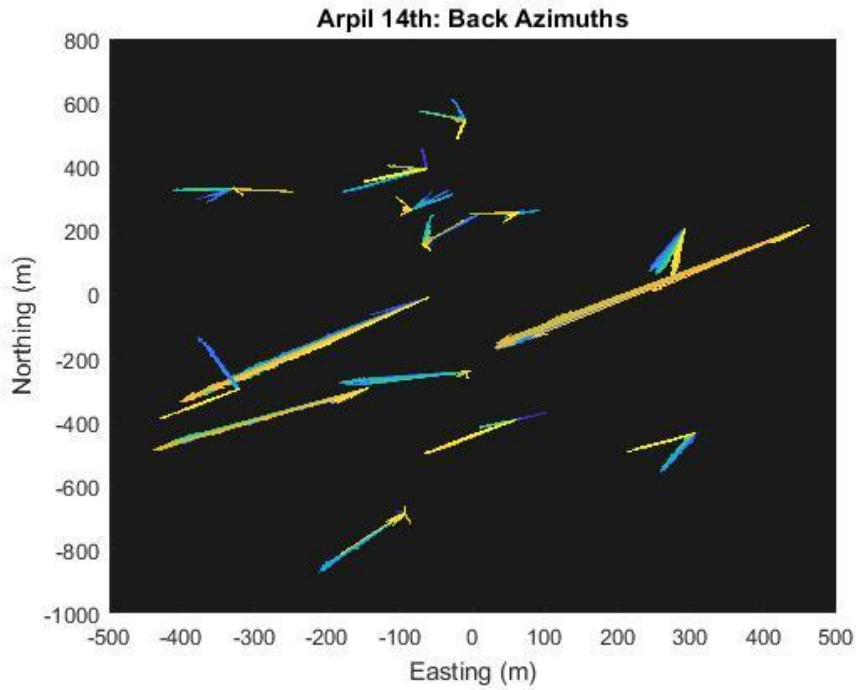

Figure 6.13: Instantaneous back azimuths from point of maximum envelope for April 14th. Variance is seen in northernmost stations with agreement of a southwest strike in southern stations.

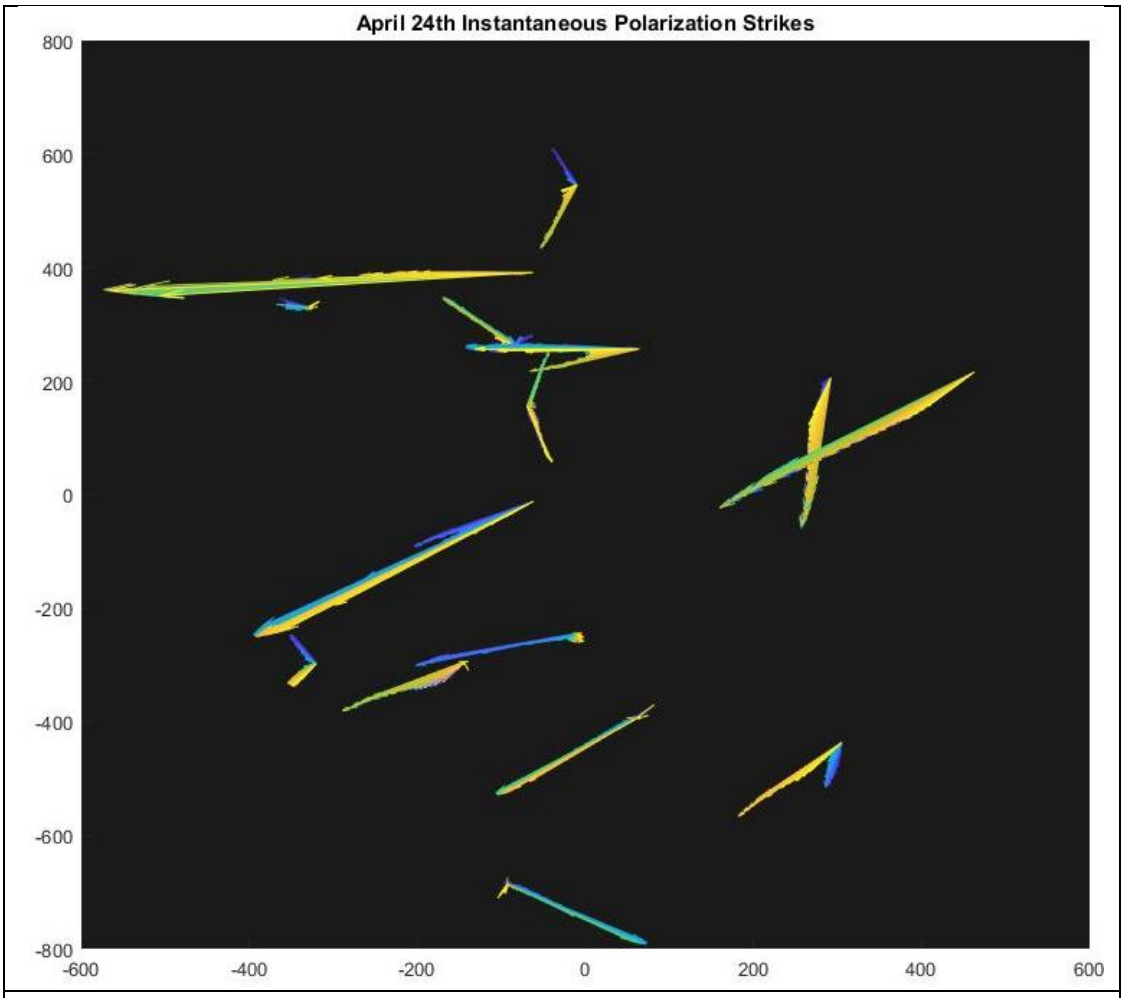

Figure 6.14: Back azimuths plotted across the array from the April 24th event. Agreement of a southwest strike is seen across stations with a variance in stations 3, 4, 12, and 13.

Source Location by Wave Arrival Time

Picking of wave onset times was guided by the best practices set forth by Deihl and Kooper, 2000, with changes in dominant FSNR and ASNR directing consistent wave onset time picking. Wave arrivals were noted to exhibit increases in dominant frequency and wave amplitude, as well as a consistent positive first motion. The seismograms plotted in **Figures 6.1, 6.2, 6.3,** and **6.4** contain red markers at the picked time of wave onset for each of the fifteen stations. A table of picked arrival times for all events can also be found within Section A of the Appendix.

Through the triangulation of apparent velocity vectors for these picked onset times, source location confidence contour maps were created. Contour confidence area was minimized with a wave velocity magnitude of 340 meters per second, thereby indicating a sound wave. **Figures 6.15a, 6.16a, 6.17a,** and **6.18a** show the generated contour maps for the April 2nd, April 9th, April 14th, and April 24th events, respectively. In these maps, contours are shaded with a color scheme that increases in confidence from yellow to black, Nodes are shown as magenta triangles, and calculated source location is shown as a green star.

On the basis of this analysis, source location for the April 2nd event has been calculated to be 332843.31 meters Easting, 4309127.93 meters Northing or Latitude and Longitude of (38.9151, -76.9280). This location in relation to the seismic array is seen in **Figure 6.15a**. **Figure 6.15b** expresses the associated misfit function which formulates regression variance for a range of source depths. When run for depths ranging from 0 to 2000 meters, with a 50 meter calculation interval, the misfit is minimized at 0 meters, indicating a source at depth 0.

As seen in **Figure 6.16a, t**he April 9th event was calculated to be sourced at the location 332823.31 meters Easting, 4309139.93 meters Northing or Latitude and Longitude of (38.9153, -76.9283). **Figure 6.16b** expresses the associated misfit function for April 9th when run for depths ranging from 0 to 2000 meters, with a 50 meter calculation interval. The misfit is minimized at 0 meters, indicating a source at depth 0.

The April 14th event was determined to have a source location of 332865.31 meters Easting, 4309189.93 meters Northing, or (Latitude, Longitude) of (38.9157, -76.9278). This location in relation to the seismic array is seen in **Figure 6.17a**. **Figure 6.17b** expresses the associated misfit function for April 14th when run for a depth range of 0 to 2000 meters, with a 50 meter calculation interval. Again, the misfit is minimized at 0 meters, indicating a surficial source.

Figure 6.18a plots source location in relation to the seismic array for the April 24th event. This event was calculated to have a source location of 332855.31 Easting, 4309167.93 Northing, or Latitude Longitude of (38.9155, -76.9279). **Figure 6.18b** shows the associated misfit function with the same depth parameters as all other event and similarly, expressing a minimized regression variance at a depth of zero.

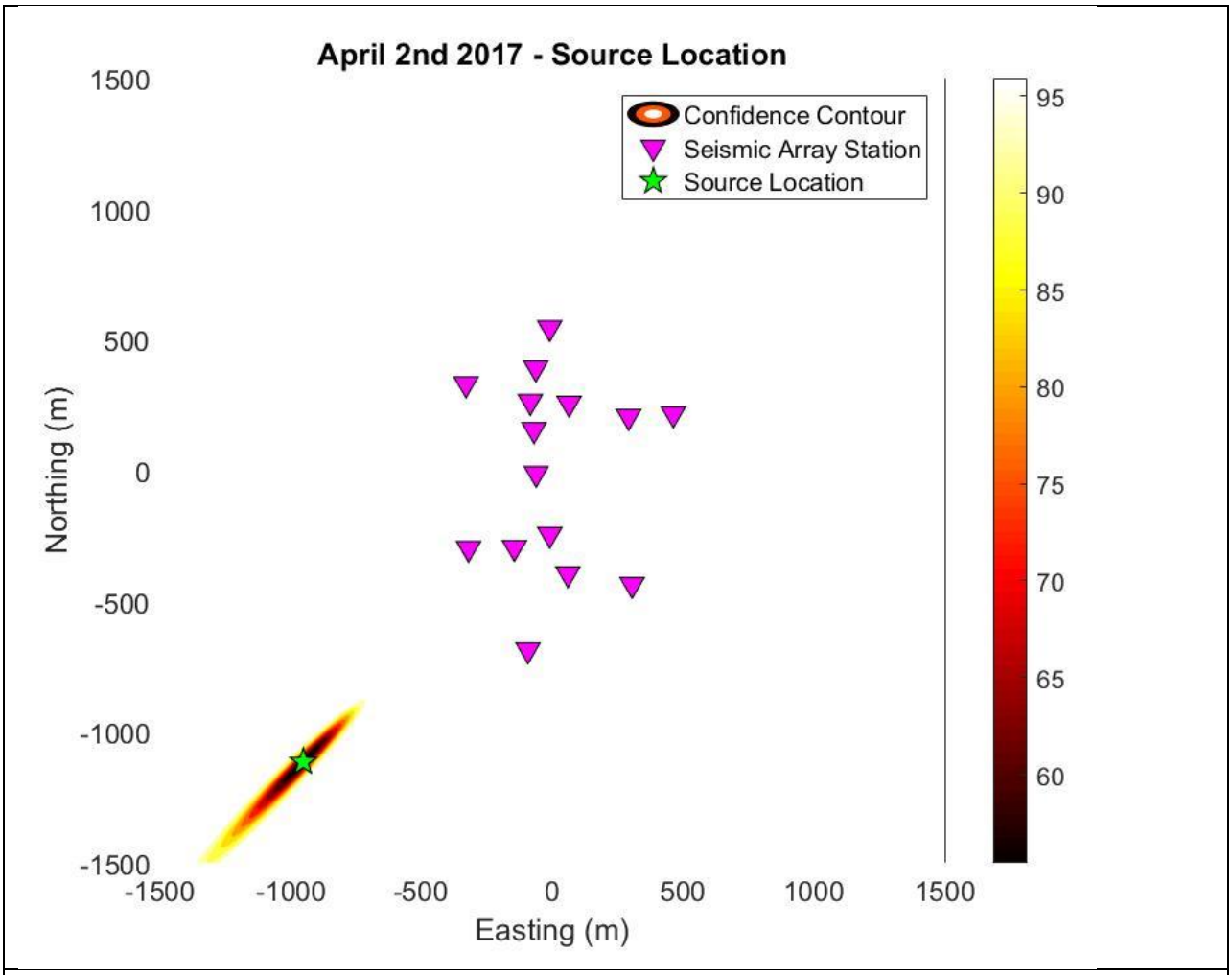

Figure 6.15a: The above confidence contour map shows calculated location with respect to the array location. Confidence intervals are color coded, nodes appear as magenta triangles, and the most confident source location is indicated by a green triangle.

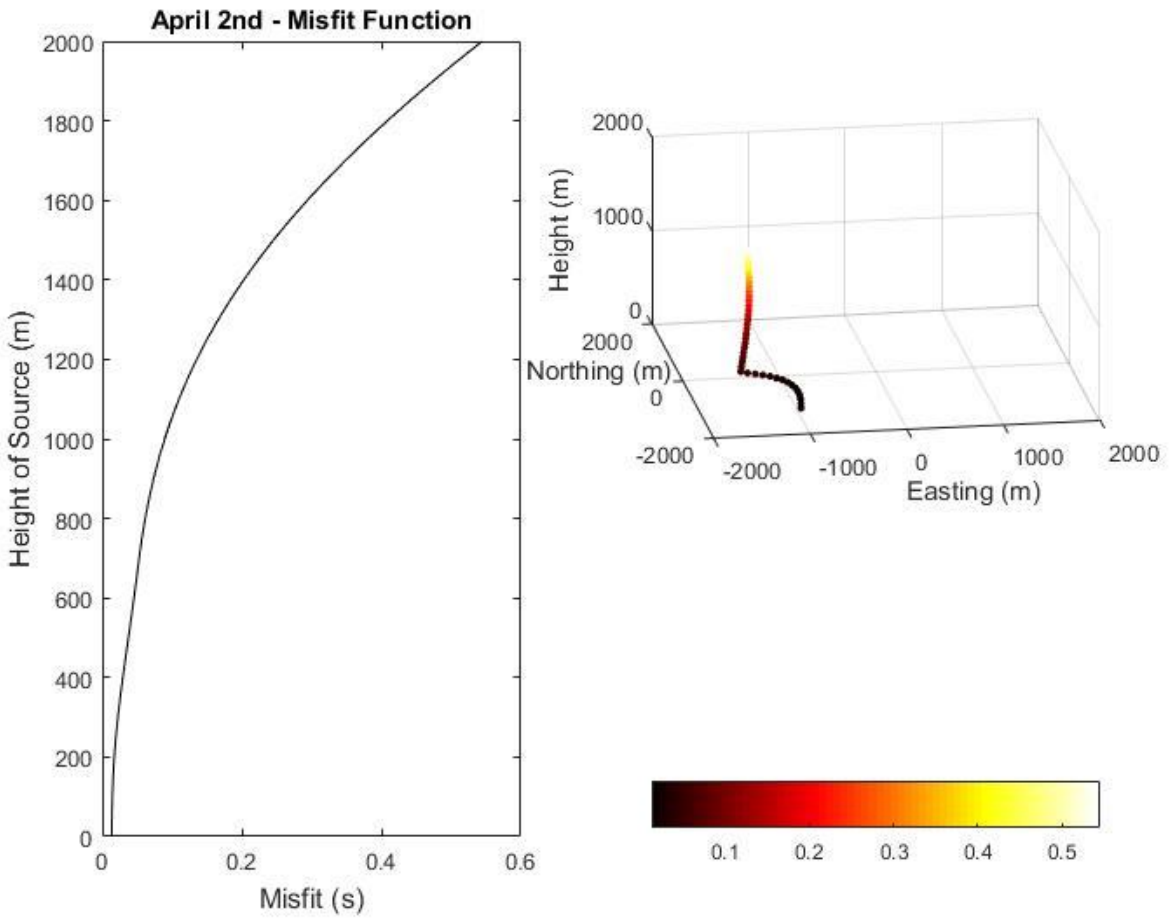

Figure 6.15b: April 2 Misfit – The above plots show that regression variance is minimized with a source depth of 0 meters, indicating a surficial source.

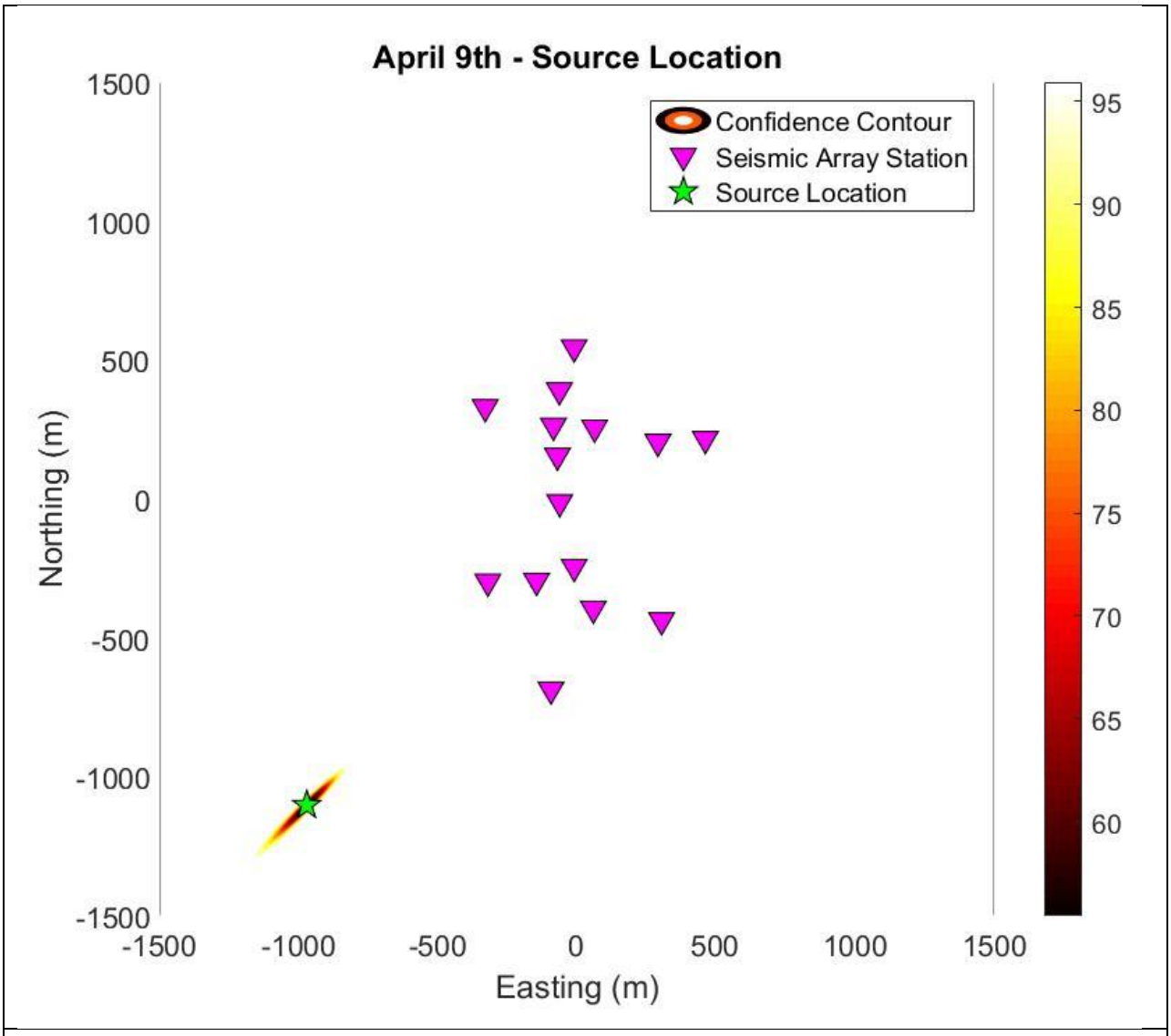

Figure 6.16a: The above confidence contour map shows calculated source location with respect to the array location. Confidence intervals are color coded, nodes appear as magenta triangles, and the most confident source location is indicated by a green triangle.

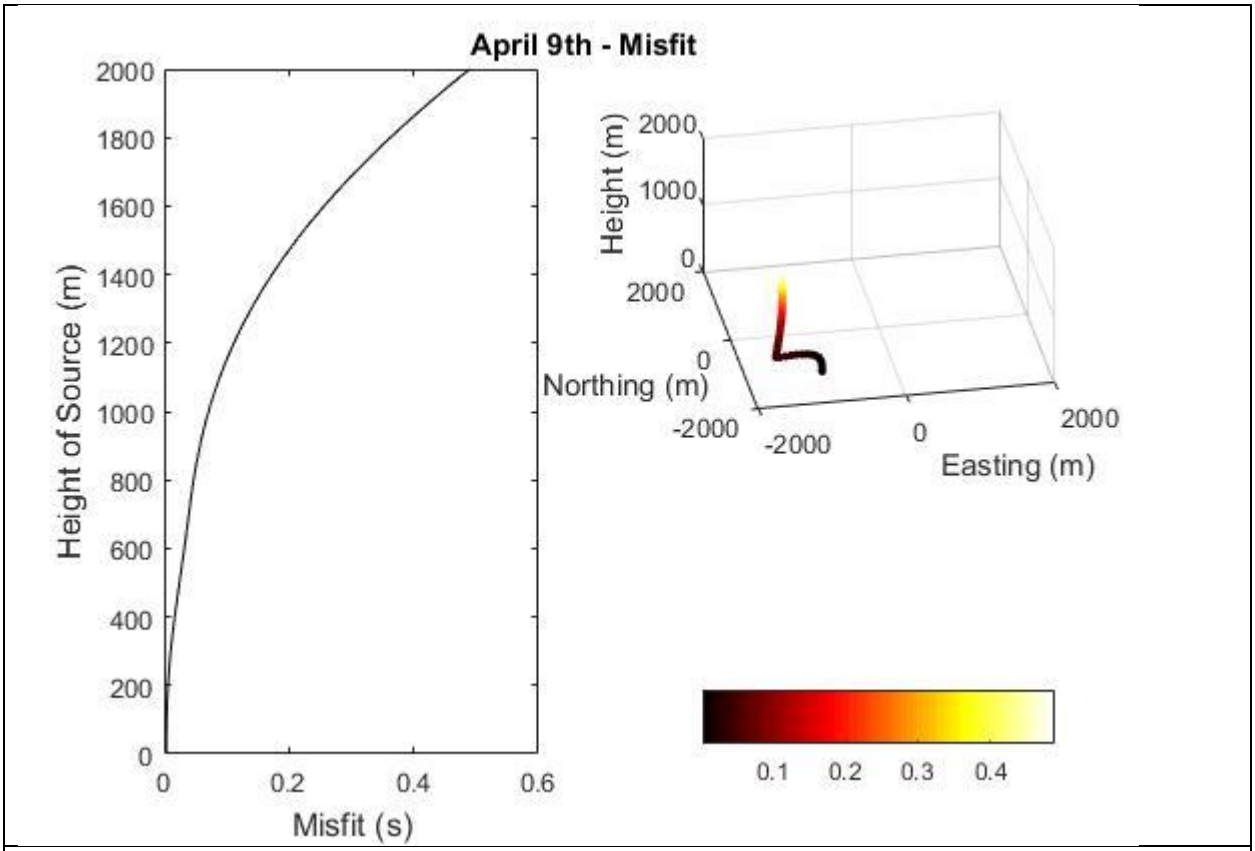

Figure 6.16b: April 9th Misfit – The above plots show that regression variance is minimized with a source depth of 0 meters, indicating a surficial source.

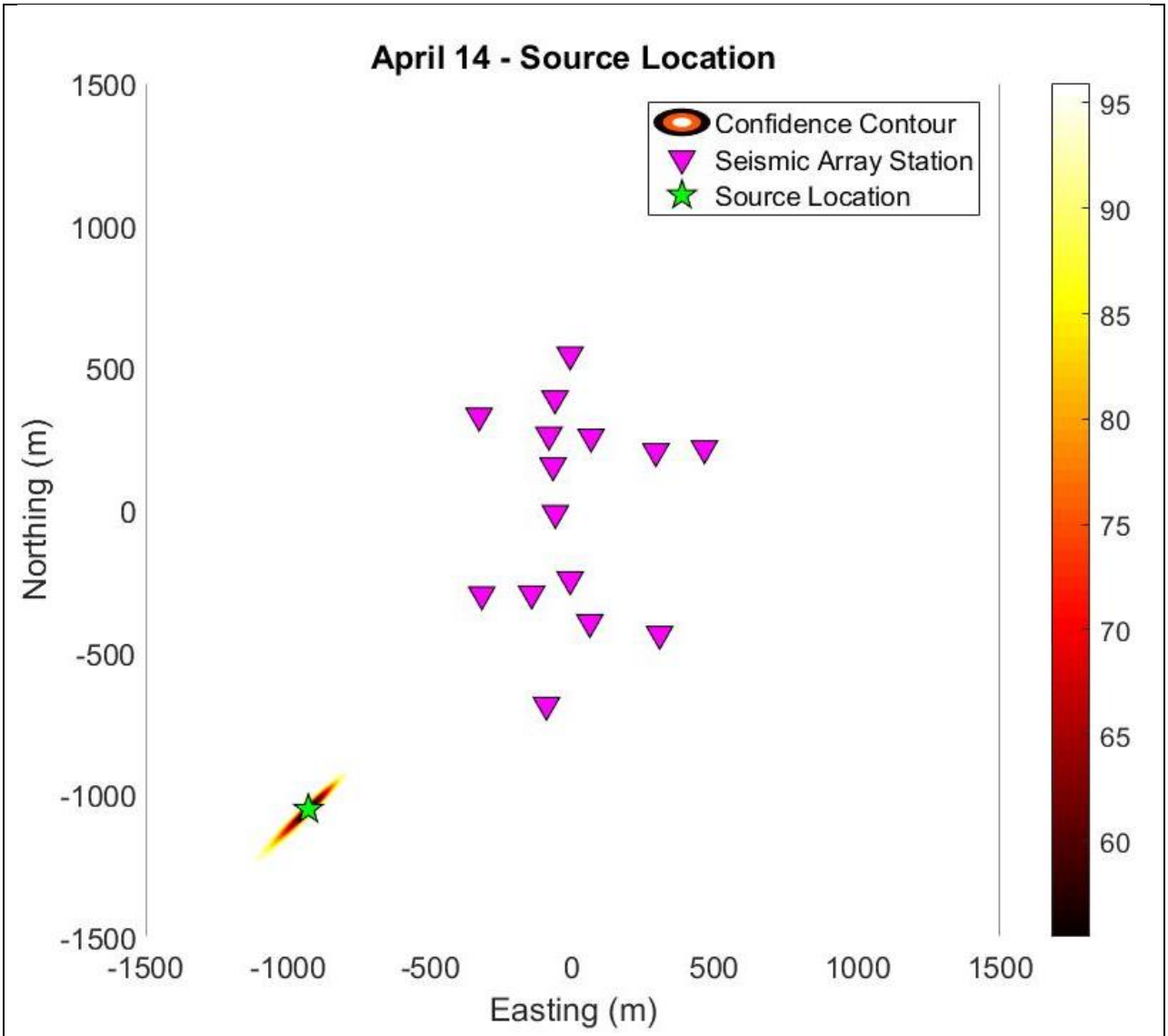

Figure 6.17a: The above confidence contour map shows calculated source location with respect to the array location. Confidence intervals are color coded, nodes appear as magenta triangles, and the most confident source location is indicated by a green triangle.

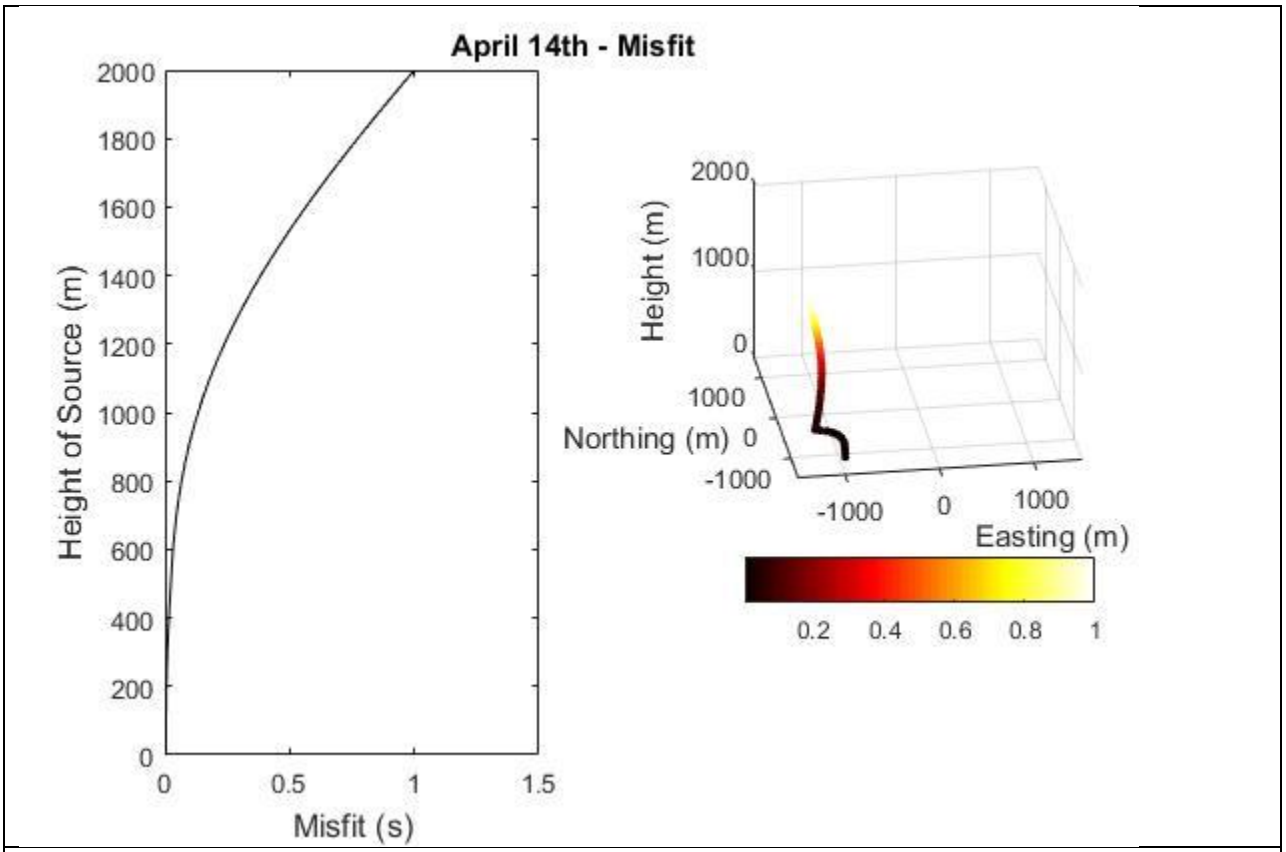

Figure 6.17b: April 14th Misfit – The above plots show that regression variance is minimized with a source depth of 0 meters, indicating a surficial source.

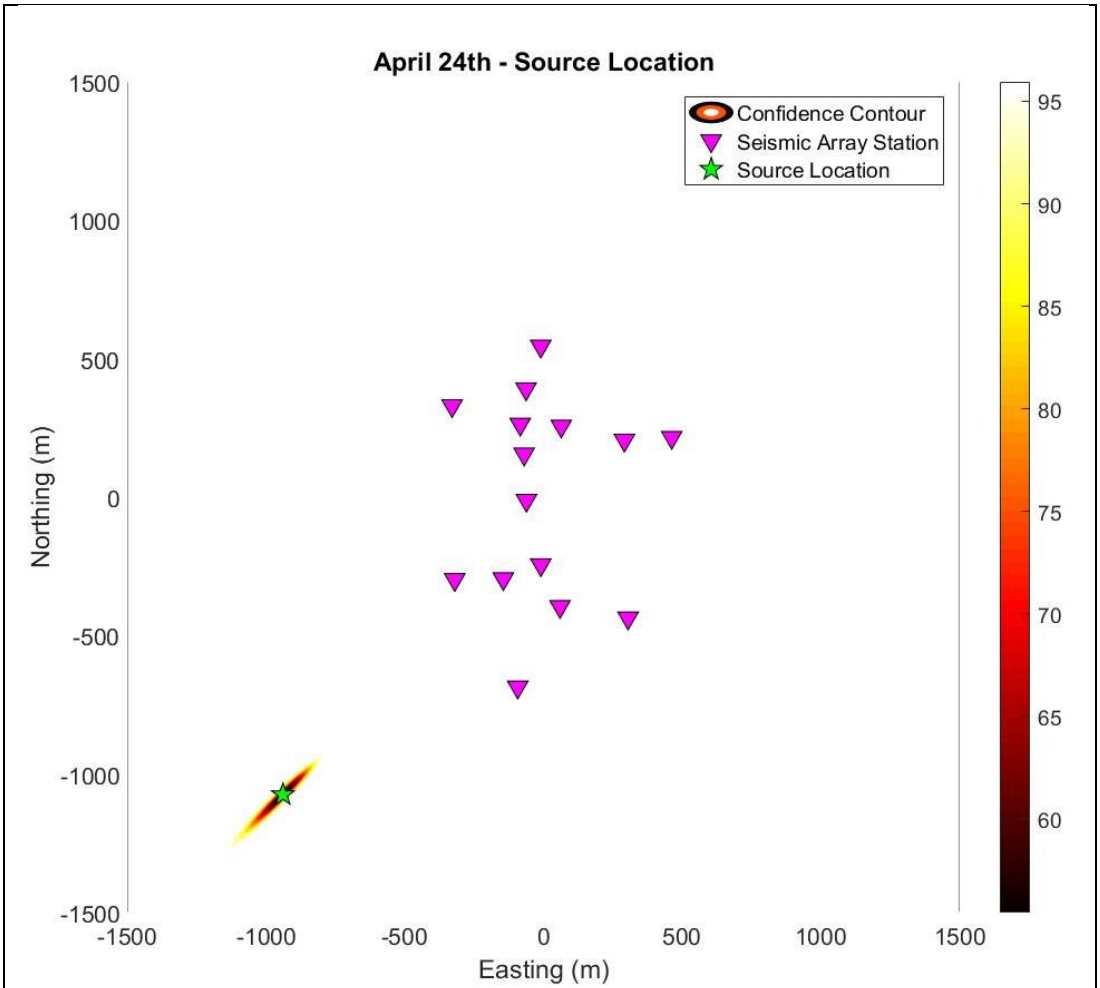

Figure 6.18a: The above confidence contour map shows calculated source location with respect to the array location. Confidence intervals are color coded, nodes appear as magenta triangles, and the most confident source location is indicated by a green triangle.

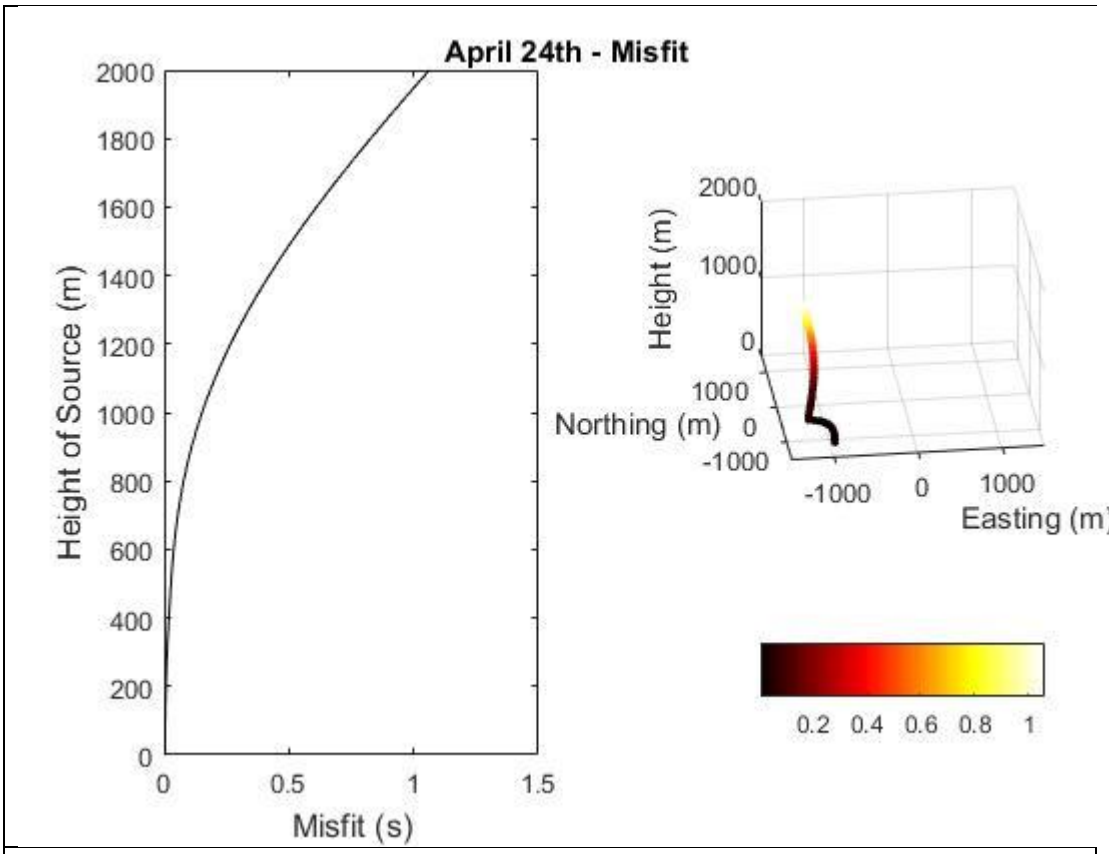

Figure 6.18b: April 24th Misfit – The above plots show that regression variance is minimized with a source depth of 0 meters, indicating a surficial source.

VII. Analysis of Uncertainty

Uncertainty of Measurement

Uncertainty within this project will be viewed in two regards, causes of uncertainty within data measurement and uncertainty within source location estimation. The first variability inducing factor of this experiment occurred within node deployment. Nodes must be oriented consistently with azimuth 0 such that components recording orthogonal vibration are aligned with X, Y, and Z axis. Field deployment utilized cell phone compasses, and as such, orientation angles are not considered precise or consistent. This factor propagated uncertainty within back azimuth calculations.

The other drivers of variability is wave onset time picking. Time of day and strength of event greatly influenced the uncertainty in picking of wave onset arrival times. Signal

strength is the characteristic which ASNR methods distinguish wave onset, and therefore, strong events see a more noticeable onset over ambient noise. Furthermore, cultural noise increases during the day hours, and causes greater ambient noise across frequencies, decreasing the observed signal to noise ratio.

Given these considerations, strong events, as seen in the spectrograms, that occur late at night or early in the morning, are likely to have least uncertainty in wave onset arrival time picking. The wave onset arrival time picks of the April 24th event are likely to contain less uncertainty due to its higher power, its wider range of frequencies, and the late hour of which it occurred. The April 2nd event contains the most uncertainty purely due to the weakness of signal and limited breadth of emitted frequencies, as seen in **Figure 6.5**. Stacked seismograms were utilized to compare waveforms between events in order to further ensure the consistency of onset times picked. The impact of these seismograms, seen in **Figure 8.3,** is discussed in Section 8.

Uncertainty of Results

The output provided by analysis have two types of uncertainty. The first of these, uncertainty in back azimuth calculations, was driven by the high frequency of data, is seen in **Figure 7.1**. This plot shows the distribution of back azimuths calculated for station 7 for the April 9th event. The plotted rose diagram shows dominant back azimuths by vector count and variability among measurement. Due to the high frequency of events, no filter could perfectly isolate the signal from high frequency cultural noise. This ambiance of high frequency noise added variability to each calculated back azimuth.

As a means of calibration, polarization back azimuths were calculated for the Kamchatka earthquake of March 29th. This event has a known epicenter at (56.938, 162.786) and as such, all back azimuths should align with the heading from Cheverly to Kamchatka, approximately -82 degrees. However, as seen in **Figure 7.2**, this is not true for all stations. Stations 3, 4, 12 and 13 vary the greatest from the true back azimuth, by up to 30 degrees. Measurements from these stations are considered to have the most uncertainty; through this confirmation of misalignment, calibration by the known Kamchatka earthquake serves to explain the greatest variability seen in back azimuth calculations as an error in data collection rather than analysis. Overall, dominant trends in back azimuth across the array align with true azimuth of -82 degrees. Therefore, the array maintains effectiveness in its ability to determine direction to source in spite of the misalignment of four stations.

Regardless of waveform similarity and consistency of onset arrival time picking, variance still exists within resultant source locations. Resultant source locations contained a standard deviation of 18 meters in UTM Easting and 25 meters in UTM Northing.

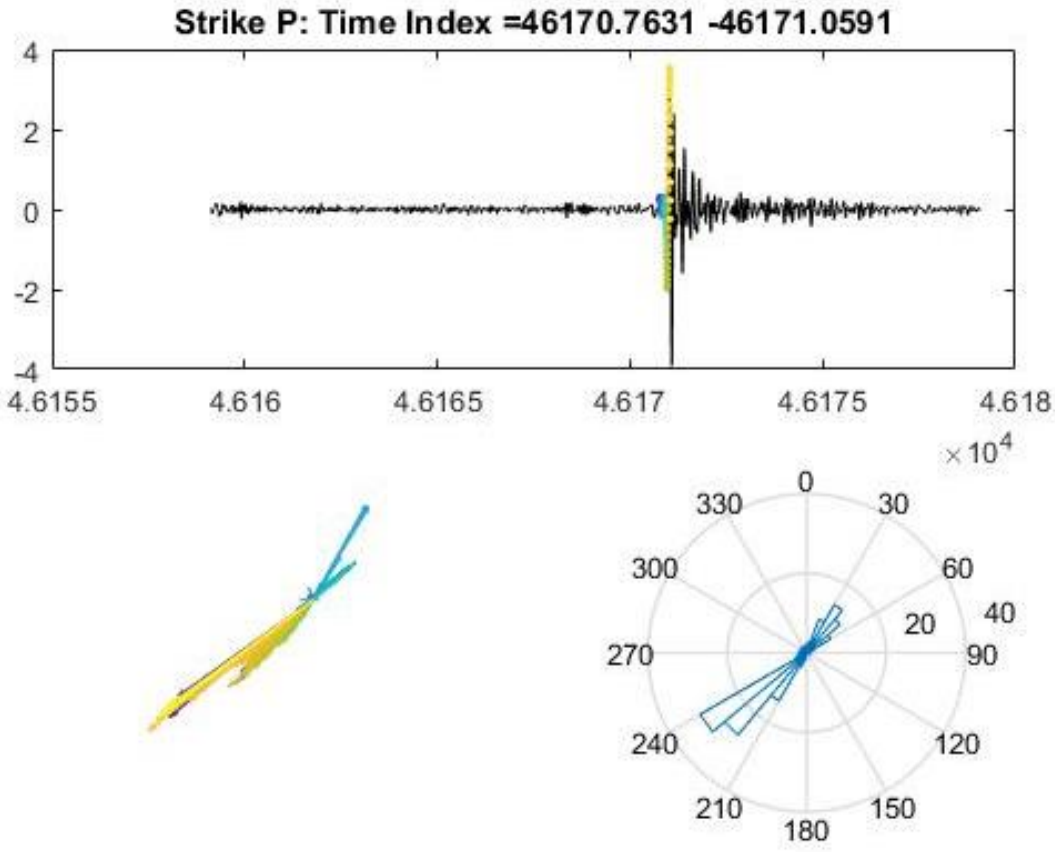

Figure 7.1: Polarization data for station 7, April 9th event. Seismogram (top) shows the selected onset interval for the calculation of back azimuths. Vector plot (left) expresses each calculated back azimuth as a vector of number of similar back azimuths, as well as color by time. The rose diagram (right) shows the distribution of back azimuths into 24 bins of 15 degrees each. A mean back azimuth of -125 (+/- 5) and its linear reciprocal are evident.

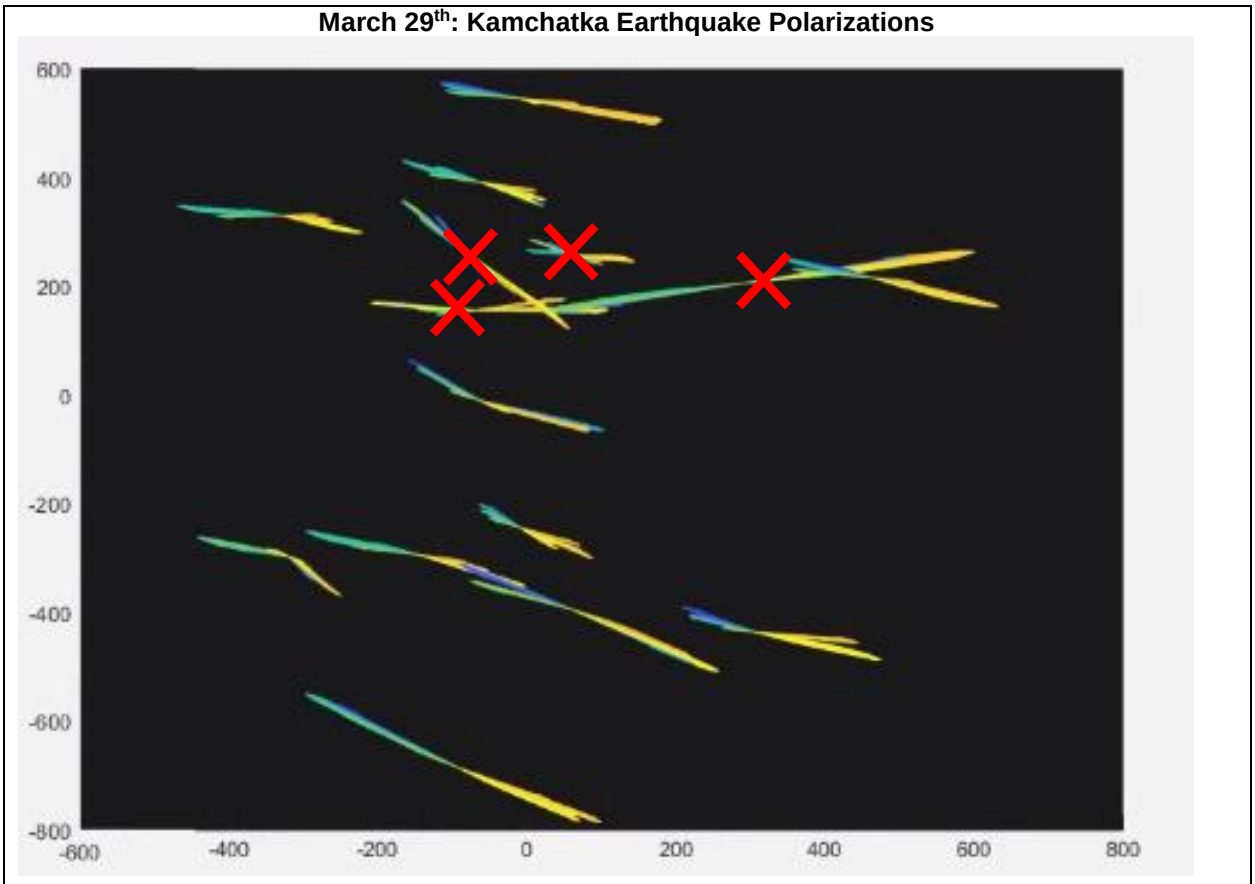

Figure 7.2: The above plot of aggregated back azimuths from the Kamchatka Earthquake of March 29th show a agreement across stations in back azimuth with major variance limited to four stations. Stations 3, 4, 12 and 13, covered by red X, demonstrate misalignment upon deployment due to their inconsistent back azimuths.

VIII. Discussion of Results

This project shows that seismic records are consistent to residential reports, as an anomalous, isolated burst in low frequency energy is observed for each reported event time. Furthermore, the plotting of vertical components from each of the 15 stations for all events, as seen in **Figure 8.1,** shows identical order of arrival across events. Furthermore, when equalized for time such that phase onset is plotted at t=0, as seen in **Figure 8.2**, signals across events are seen to have congruent waveform with a consistent positive first motion. This phase arrival consistency, compounded with congruent waveform between events, and maximum spectral power of 7 Hz, is compelling evidence that all events originate from the same source.

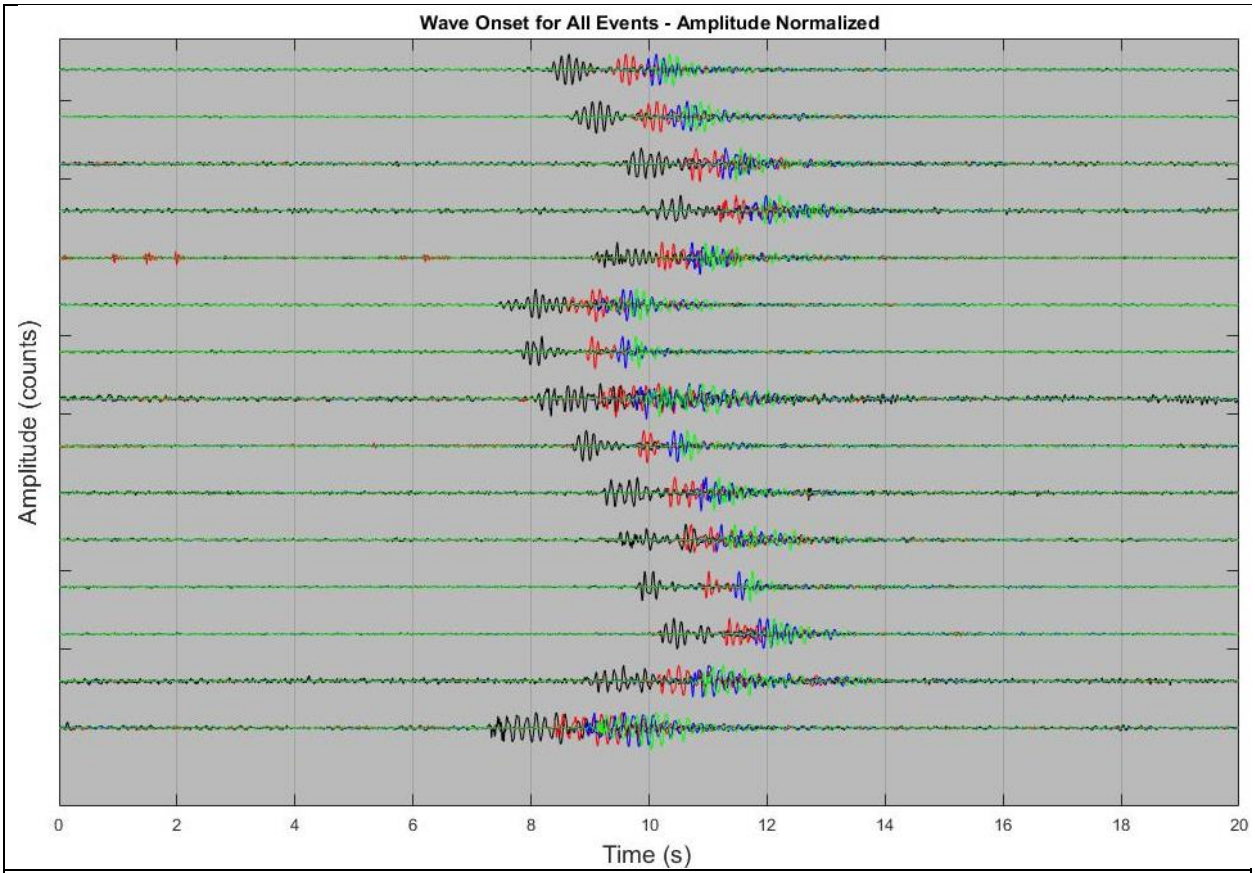

Figure 8.1: The above plot exhibits the superposition of seismograms for all events with normalized amplitude for the comparison of arrival order. Seismograms of the April 2nd event are shown in black, the April 9th event are shown in red, the April 14th event are shown in green and the April 24th event are shown in Green.

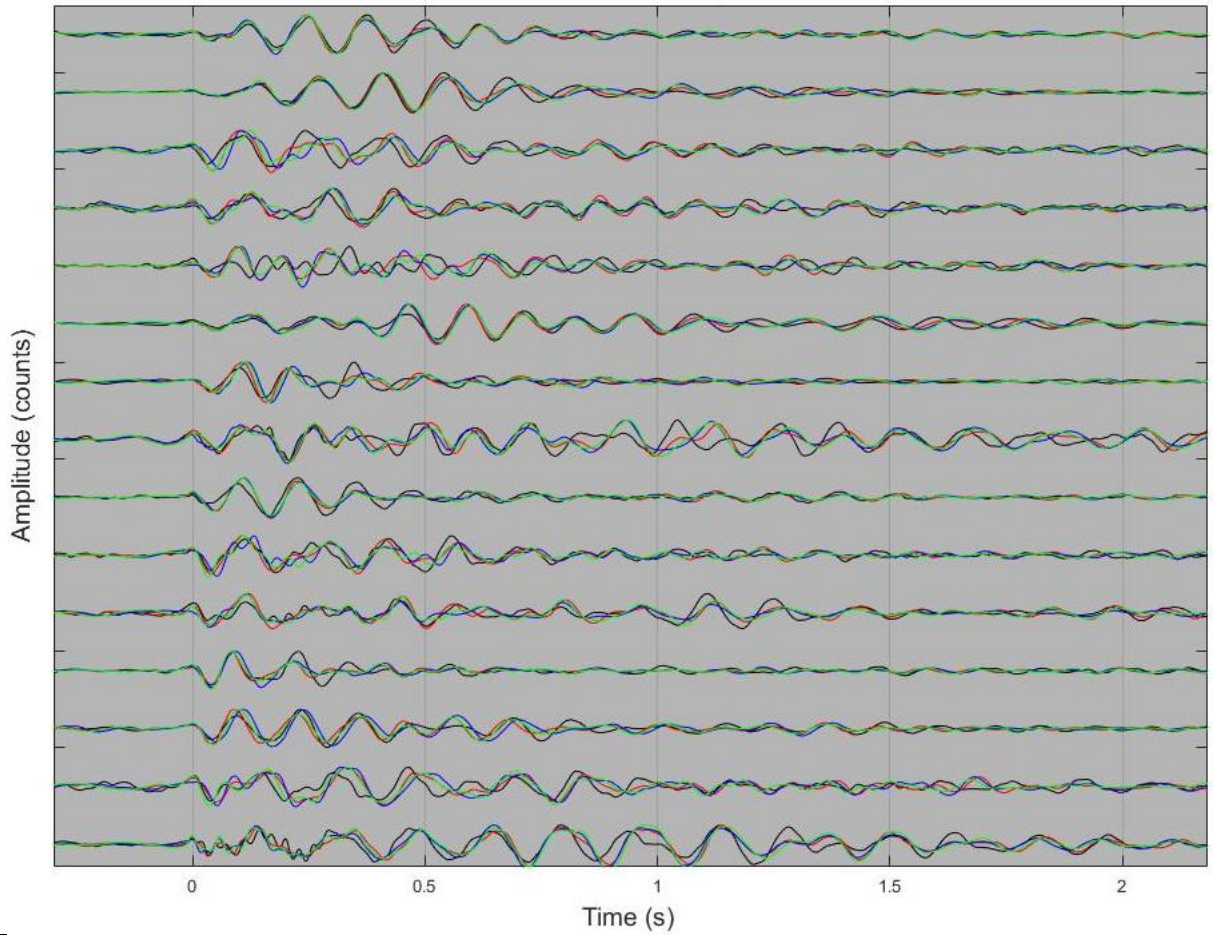

Figure 8.2: The above stacked seismograms demonstrate the congruence of waveform across events. Stations 1-15 are plotted from top to bottom with April 2nd, 9th, 14th, and 24th events in black, red, blue, and green respectively. Wave form is seen to maintain consistency between events, indicating singularity of source.

The evaluation of source location finds agreement between particle polarization during wave onset, and source locations calculated on the basis of arrival times. The compilation of these source locations results in a mean source location of 332846.81 meters Easting, 4309156.43 meters Northing or coordinates (38.9154, -76.9279).

Figure 8.3 Shows the mean source location plotted relative to local geography with the town of Cheverly identifiable in the upper right and the mean source location shown as a green circle. This mean point of origin is found to reside beyond the residential bounds of the Town of Cheverly as identified within zoning by the Prince George's Planning Department. When all events are plotted relative to geography with events as yellow circles and mean as a green circle as seen in **Figure 8.4**, all events are found to reside within one property. This property belongs to the scrap and recycling company of Joseph Smith and Sons Inc – Professional Services, of Capitol Heights, MD.

Figure 8.3: Mean source location plotted as a green circle shows booms to be emitted from beyond the residential bounds of Cheverly.

Figure 8.4: The origin of all events plotted as yellow circles with the mean as a green circle. The origin of all events are found to reside within the bounds of Joseph Smith and Son's – Professional Services Inc. This plot exhibits the precision of location estimations, driven by consistency in time picking methods.

IX. Suggestions of Future Work

The data collected for this project have great potential as they are expansive and unique in nature. The reduced aperture of the array enables greater visibility of high frequency noise. Prominent signatures of planes, trains, and automobiles were observed throughout the seismic record, the high frequency visibility may lend to the formal characterization of these sources of cultural noise. Fuchs et al 2017, have already commenced a similar study on train induced vibration. Studies of the same nature will but directed towards other sources of cultural noise such as cars, will be possible.

Additionally, there is a possibility for cross correlation analysis, in which more expansive durations of the seismic record are screened for the signature of a boom. This follow up

would leverage the congruence of waveforms between events in order to identify possibly unreported booms. Such an analysis may shed light on periodicity of events.

Finally, similar arrays have been and are currently deployed by the University of Maryland Seismological Laboratory for the evaluation of hydrologic systems. The data recorded by this project's array may be viewed in parallel to other arrays for a wider geographic distribution of nodes.

X. Conclusions

There is startling consistency between the arrival time, waveform, and spectral character of each of the four observed events. The congruency of waveform and arrival time within seismograms are early indicators that all four events originated from the same source. Strong waveform similarity has been used to indicate source locations within ¼ of the dominant wavelength (e.g. Geller & Mueller, 1980). Given dominant period of 1/7 s and wavespeed of ~340m/s, this would indicate source locations less than 12 meters removed of one another.

Polarization analysis provides guiding direction to source, with consistent back azimuth calculations to the south south-west of Cheverly. Though uncertainty in the alignment of seismometers proves too great to pinpoint location on the basis of calculated back azimuth alone, calibration with the known seismic event on March 29th validate the generalized back azimuth ranging from -120 to -165 degrees.

The results of location by time picking analysis are inconsistent with the propagation of ground waves. Such activity would be expected at to originate at depth with propagation speed of at least 2000m/s (Bourbie et al., 1987), however all misfit functions are minimized at the surface, and optimized wave velocity is found to be 340 m/s. Furthermore, identical positive first motion across the array are inconsistent with the asymmetric displacement associated with slip, and more consistent with an isometric sound event. Given these considerations, the initial hypothesis that Cheverly booms are the manifestation of low magnitude shallow seismic activity is rejected on account of surficial source depth, inconsistent wave velocity, and isometric first motion.

Wave onset time picking methods for each event indicate consistent source location at within 1500 meters of Cheverly at an azimuth of -134 (± 10) degrees. Consistent phase arrival picking drove limited variance within location results, ultimately yielding a mean

source location at coordinates (38.9154, -76.9279). Mean source location, as well as all calculated source locations were found to reside within the bounds of Joseph Smith & Sons – professional services.

Surficial source depth, wave velocity aligning with that of a sound wave propagating through air, and isometric first motions seen in seismograms are consistent with sound emitted by a human driven source. Congruence of waveform across events compounded with the agreement between polarization analysis and arrival time based locating methods provide a well constrained source location with little variance. Given that results from all methods of analysis are consistent with an anthropogenic sound originating from the recycling facility to the southwest of Cheverly, the secondary hypothesis unable to be falsified. The compelling nature of the presented evidence motivates this paper to advise that the Town of Cheverly investigate the operations of Joseph Smith and Son's – Professional Services of Capitol Heights, Maryland, in order to resolve noise disturbances.

Acknowledgements

This project could not have been completed without the involvement of many from the University of Maryland Seismological Laboratory.

My many thanks to Vedran Lekic for providing constant advising, contextual insight, MatLab scripts, and writing guidance; Phillip Goodling for extensive work in the functional operation and deployment of the seismic nodal system; Nicholas Schmerr for advising deployment strategy and providing codes for analysis.

Appendix

Section A

Picked Wave Arrival Times in Seconds

Station	April 2nd	April 9th	April 14th	April 24th
1	1023.265645	46171.36078	2208.873881	13680.10239
2	1023.630532	46171.72086	2209.230006	13680.45998
3	1024.622858	46172.69031	2210.189566	13681.43319
4	1025.101793	46173.17227	2210.677589	13681.91792
5	1024.123249	46172.12249	2209.625701	13680.85523
6	1022.4866	46170.5769	2208.095682	13679.31525
7	1022.834603	46170.92591	2208.432022	13679.66203
8	1023.130923	46171.22782	2208.751875	13679.97151
9	1023.70978	46171.80118	2209.312443	13680.54201
10	1024.243844	46172.32746	2209.831315	13681.0715
11	1024.516045	46172.59613	2210.110134	13681.33997
12	1024.843374	46172.92852	2210.432976	13681.67183
13	1025.187932	46173.27198	2210.766824	13682.01487
14	1024.102576	46172.16957	2209.688353	13680.92235
15	1022.293648	46170.4024	2207.934106	13679.14746

Appendix

Section B

Honor Code:

I pledge on my honor that I have not given or received any unauthorized assistance on this assignment.

Signature:

Date: 11/22/2017

Bibliography

Ari, Ben-Menahem, and Sarra Jit Singh. *Seismic waves and sources*. (1981): 1108.

Boatwright, J., & Fletcher, J. B. (1984). *The partition of radiated energy between P and S waves.* Bulletin of the Seismological Society of America, *74*(2), 361-376.

Bourbie, T., Coussy, O., & Zinszner, B. (1987). *Acoustics of porous media*: Institut Francais du Petrole Publications.

Capon, J. A. C. K. (1973). *Signal processing and frequency-wavenumber spectrum analysis for a large aperture seismic array*. Methods in Computational Physics (Elsevier, *1973)*, *13*, 1-59.

Chunchuzov, I., Kulichkov, S., Popov, O., & Hedlin, M. (2014). *Modeling propagation of infrasound signals observed by a dense seismic network*. The Journal of the Acoustical Society of America, *135*(1), 38-48.

Davies, D., E. J. Kelly, and J. R. Filson, *Vespa process for analysis of seismic signals*, Nature Phys. Sci., 232, 8–13, 1971.

Douglas, A., Bowers, D., Marshall, P. D., Young, J. B., Porter, D., & Wallis, N. J. (1999). *Putting nuclear-test monitoring to the test*. Nature, *398*(6727), 474-475.

Ebel, J. E. (1989). *A comparison of the 1981, 1982, 1986 and 1987–1988 microearthquake swarms at Moodus, Connecticut*. Seismological Research Letters, *60*(4), 177-184.

Fuchs, Florian, and Götz Bokelmann. *Broadband seismic effects from train vibrations*. EGU General Assembly Conference Abstracts. Vol. 19. 2017.

Geller, R. J., and C. S. Mueller (1980). *Four similar earthquakes in central California*, Geophys. Res. Lett. 7, 821–824.

Glaser, John D. *Geologic Map of Prince Georges County, Maryland:* Maryland Geologic Survey. http://www.mgs.md.gov/maps/PGGEO2003_2_S83.pdf., 2006

Heffner, H. E., & Heffner, R. S. (2007). *Hearing ranges of laboratory animals.* Journal of the American Association for Laboratory Animal Science, *46*(1), 20-22.

Hill, D., Fischer, F., Lahr, K,. Coakley, J. *Earthquake Sounds Generated by Body-wave Ground Motion:* Bulletin of the Seismological Society of America August 1976 vol. 66 no. 4 1159-1172. http://citeseerx.ist.psu.edu/viewdoc/download?doi=10.1.1.849.6444, Web.

Hill, D. P. (2011). *What is That Mysterious Booming Sound?*. Seismological Research Letters, *82*(5), 619-622. Web.

Husebye, E. S., & Ruud, B. O. (1989). *Array seismology—Past, present and future developments*. Observatory Seismology, 123-153.

Ingate, S. F., Husebye, E. S., & Christoffersson, A. (1985). *Regional arrays and optimum data processing schemes.* Bulletin of the Seismological Society of America, *75*(4), 1155-1177.

Kilb, D., Peng, Z., Simpson, D., Michael, A., Fisher, M., & Rohrlick, D. (2012). Listen, watch, learn: SeisSound video products. Seismological Research Letters, *83*(2), 281-286.

Koper, Keith D., Terry C. Wallace, and Richard C. Aster. *Seismic recordings of the Carlsbad, New Mexico, pipeline explosion of 19 August 2000*. Bulletin of the Seismological Society of America 93.4 (2003): 1427-1432.

Lawson, A. C., & Reid, H. F. (1908). *The California Earthquake of April 18, 1906: Report of the State Earthquake Investigation Commission..* (No. 87). Carnegie institution of Washington.

Michael, A. J. (2011). Earthquake sounds. In *Encyclopedia of solid earth geophysics* (pp. 188-192). Springer Netherlands.

Morozov, Igor B., and Scott B. Smithson. *Instantaneous polarization attributes and directional filtering.* Geophysics 61.3 (1996): 872-881

Peterson, J. (1993). Observations and modeling of seismic background noise.

Rost, S., and C. Thomas, *Array seismology: Methods and applications*, Rev. Geophys., 40(3), 1008, doi:10.1029/2000RG000100, 2002.

Town of Cheverly, *Welcome to Cheverly*, Published 2012. Access March 29th, 2017, web. *:* http://www.cheverly.com/Pages/index, Web.

The Maryland-National Capital Park and Planning Commission, *The Preliminary Greater Cheverly Sector Plan,* January 2017. http://www.mncppcapps.org/planning/Publications/PDFs/319/Preliminary%20Greater%20Cheverly%20Sector%20Plan.pdf Web.

Wood, H. O., & Neumann, F. (1931). *Modified Mercalli Intensity Scale of 1931*. Seismological Society of America.